Title

Characterization of transgenic mouse models targeting neuromodulatory systems reveals organizational principles of the dorsal raphe

Journal

Nature Communications, 10(1)

ISSN

2041-1723

Authors

Cardozo Pinto, Daniel F
Yang, Hongbin
Pollak Dorocic, Iskra
et al.

Publication Date

2019

DOI

10.1038/s41467-019-12392-2

Peer reviewed

Diversity of transgenic mouse models targeting neuromodulatory systems reveals anatomical and functional heterogeneity of the dorsal raphe

Daniel F. Cardozo Pinto[1,4], Hongbin Yang[1], Vivian J. Han[1], Iskra Pollak Dorocic[1], James R. Peck[1], Kevin T. Beier[2], Marten P. Smidt[3] and Stephan Lammel[1,5,*]

[1]Department of Molecular and Cell Biology and Helen Wills Neuroscience Institute, University of California Berkeley, Berkeley, CA 94720, USA

[2]Departments of Physiology and Biophysics, University of California Irvine, Irvine, CA 92697, USA

[3]Swammerdam Institute for Life Sciences, FNWI University of Amsterdam, The Netherlands

[4]Current address: Department of Psychiatry and Behavioral Sciences, Stanford University, Stanford, CA 94305, USA

[5]Lead Contact

*Correspondence:

Stephan Lammel, Ph.D.
Department of Molecular and Cell Biology
and Helen Wills Neuroscience Institute
142 Life Science Addition #3200
University of California Berkeley
Berkeley, CA 94720, USA
Phone: 510-664-7821
E-Mail: lammel@berkeley.edu

ABSTRACT

The dorsal raphe nucleus (DR) is a heterogeneous brain region containing dopamine (DA), serotonin (5HT), γ-aminobutyric acid (GABA) and glutamate neurons. While transgenic mouse lines have proven to be a critical tool for manipulating DR neurons, the complexity of this nucleus requires Cre-driver lines that restrict transgene expression to a precisely defined target population. Here, we carried out a systematic evaluation of the cell-type specificity of five Cre-driver lines targeting neuromodulatory populations in the DR. We find dramatic differences in cell-type specificity between lines targeting DA neurons, and a two-fold difference in penetrance between lines targeting 5HT neurons. Using these mouse lines, we map genetically-defined DR circuits and show that neurochemically distinct populations of DR neurons are arranged in topographical pattern, send divergent projections to amygdala subnuclei, and differ in their presynaptic inputs. Strikingly, targeting the same cell population using different Cre-driver mouse lines yielded both structural and functional differences in the neural circuits accessed. Our results provide a refined model of DR circuitry, illustrate the importance of comparative analyses between transgenic lines for the interpretation of optogenetic experiments, and support a case-by-case evaluation of the suitability of any mouse line for a given experimental application.

MAIN TEXT

INTRODUCTION

Transgenic mouse lines expressing Cre-recombinase under the control of specific promoters have revolutionized neuroscience by facilitating genetic access to defined cell groups of the mammalian brain. In addition to their original utility for generating tissue specific gene knock-outs, Cre-driver lines have been integrated with a proliferating library of viral vectors and genetically encodable fluorescent tags, opsins, and calcium indicators to become ubiquitous tools for labeling, manipulating, and recording from neural circuits. The application of these mouse lines to the study of neuromodulatory systems has been particularly productive because they provide a handle onto DA, 5HT, noradrenaline, or acetylcholine neurons (among others) that are interspersed among other cell-types in heterogeneous subcortical nuclei[1–6]. A prominent branch of this work has focused on the midbrain dopamine (DA) system accessed via mouse lines expressing Cre under the control of promoters for the biosynthetic enzyme tyrosine hydroxylase (TH-Cre) or the DA

transporter (DAT-Cre). Importantly, the choice of Cre-driver mouse line proved to be critical for the interpretation of supposedly DA-specific optogenetic experiments in the ventral tegmental area (VTA) as TH-Cre, but not DAT-Cre, mice were shown to induce transgene expression in numerous cells in and around the VTA that lack detectable levels of TH protein and therefore may not be *bona fide* DA neurons[7,8].

More recently, there has been intense interest in the application of Cre-driver lines to study neuromodulatory populations in the nearby dorsal raphe nucleus (DR) whose organization and function are only beginning to be understood. The DR is best known for its large population of serotonin (5HT) neurons that can be accessed with transgenic mouse lines expressing Cre under the promoter of the serotonin transporter (SERT-Cre) or the enhancer of the transcription factor PET1 (ePET-Cre)[3,6,9,10]. These neurons send broadly collateralizing axons to nearly all regions of the forebrain[11,12] and have been shown to play a role in behaviors as distinct as locomotion[12–14], reward[15–17], anxiety[18], allodynia[19] and social interaction[20,21]. Interestingly, reports of their functions in some of these behaviors have been conflicting. For example, while some groups have found that activating DR 5HT neurons is reinforcing[16] and suppresses locomotion[12], others have reported the absence of these effects[21–24], and still others have proposed that DR 5HT neurons can facilitate or suppress locomotion in a state dependent manner[25]. In addition, DR 5HT neurons show dynamic changes in their firing patterns in response to motivational stimuli on multiple timescales[22,24,26], possibly representing the underlying dynamics of their various inputs[27–29]. A compelling explanation for some of these inconsistencies could be differential recruitment of functionally distinct subpopulations of DR 5HT neurons, and indeed two projection-defined subsystems of DR 5HT neurons that differ by their expression vesicular glutamate transporter VGluT3 (*Slc17a8*) have recently been described[12,30]. Considering that known projection targets of DR 5HT neurons such as the striatum are not represented in this two-system model though, further heterogeneity and complexity in the DR 5HT neuron population is likely to exist. In addition to 5HT neurons, the DR also contains DA neurons[31]. DR DA neurons represent a continuous population with the sparse DA neurons of the periaqueductal gray (PAG), and they are known to project to the central amygdala (CeA) and bed nucleus of the stria terminalis (BNST)[32–35]. In the last few years, several studies have established roles for DR DA neurons in pain related behaviors[34,36], social isolation and aversion[35], arousal and sleep[32], and associative fear learning[37]. Based on the well-established heterogeneity of VTA DA neurons[38–40], projection-defined and functionally distinct DR DA subpopulations may explain the diverse functional roles of these neurons in seemingly disparate behaviors. In the

case of DR DA neurons, however, the input/output relationships underlying specific behavioral functions remain largely unknown.

Recognizing that future investigations of these DR neuromodulatory systems will depend critically on Cre-driver lines and motivated by the discovery of off-target effects in a mouse line used to study VTA DA neurons[7], we have carried out a comparative analysis of the cell-type specificity of five transgenic mouse lines used to target DR 5HT or DA neurons. We find dramatic differences in cell-type specificity between DA-targeting lines (TH-Cre, DAT-Cre, PITX3-Cre), and a two-fold difference in penetrance between 5HT-targeting lines (SERT-Cre, ePET-Cre). Furthermore, we used these mouse lines to reveal that genetically-defined DR subpopulations are anatomically segregated and differ in their afferent and efferent connections. Finally, we show that targeting the same cell population with different mouse lines produces systematic structural and functional differences in the neural circuits accessed as defined by quantitative differences in their presynaptic inputs and differential co-transmission of glutamate and dopamine. We thereby propose a refined model for the structure of the DR and its associated circuitries and advocate in favor of a case-by-case evaluation of the suitability of a Cre-driver mouse line for any given brain region and application.

RESULTS

Anatomical characterization of transgenic mouse lines for targeting DR 5HT and DA neurons

We first carried out a systematic evaluation of the cell-type specificity of five transgenic mouse lines used to target 5HT and DA systems in the DR (**Fig. 1a**). With regard to the 5HT system, we examined the SERT-Cre[3] and ePET-Cre[10] mouse lines which drive Cre expression under control of the serotonin transporter gene (*Slc6a4*; SERT) or the enhancer of the *Fev* gene, a transcription factor expressed in 5HT neurons, respectively. In the case of the DA system, we characterized the DAT-Cre[41], TH-Cre[42] and PITX3-Cre[43] mouse lines which drive Cre expression under control of the dopamine transporter (*DAT*), tyrosine hydroxylase (*TH*) or *PITX3* genes, respectively. The *PITX3* gene codes for a transcription factor known to play a role in the differentiation of midbrain DA neurons and transgenic lines driven by its promoter have previously been used to study the DA system[31,35,43,44].

To analyze the cell-type specificity of transgene expression in the DR of SERT-Cre and ePET-Cre mice targeting 5HT neurons, we injected a Cre-dependent adeno-associated

virus encoding enhanced yellow fluorescent protein (1 µl AAV5-DIO-eYFP, ~10^{12} infectious units/ml) into the DR. We then divided the DR into four subregions and systematically analyzed co-localization of eYFP with immunohistochemically-detected tryptophan hydroxylase 2 (TpH) protein; the rate limiting enzyme in the biosynthesis of 5HT (**Fig. 1b, e**). Co-localization between eYFP and TpH was high across all four subregions in both SERT-Cre and ePET-Cre mice (SERT-Cre: eYFP+/TpH+ 95.2%, n = 818/862 cells from n = 3 mice; ePET-Cre: eYFP+/TpH+ 87%, n = 360/414 cells from n = 3 mice). Notably though, we found that the SERT-Cre line labeled approximately twice as many TpH+ neurons compared to the ePET-Cre line in mice that received identically targeted injections and equivalent injection volumes (**Fig. 1c, d, f, g**). This trend was consistent across all animals studied. To confirm that this difference in labeling was not due to random differences in the diffusion of the viral solution, we injected separate cohorts of SERT-Cre and ePET-Cre mice with AAV5-DIO-eYFP (1 µl AAV-DIO-eYFP, ~10^{12} infectious units/ml) into the median raphe (MnR); a second major serotonergic nucleus (**Supplementary Fig. 1A, E**). Immunohistochemical analysis revealed a slightly lower selectivity for transgene expression in TpH-positive neurons compared to the DR for both lines (SERT-Cre: eYFP+/TpH+ 85.8%, n = 641/747 cells from n = 3 mice; ePET-Cre: eYFP+/TpH+ 78%, n = 160/205 cells from n = 3 mice), but again we observed much higher labeling for TpH+ neurons in SERT-Cre compared to ePET-Cre mice (**Supplementary Fig. 1B-D, F-H**). Overall, these data indicate that while the cell-type specificities of the SERT-Cre and ePET-Cre mouse lines are comparable, the penetrance of transgene expression between them is dramatically different.

Next, we injected AAV-DIO-eYFP into the DR of DAT-Cre, TH-Cre and PITX3-Cre mice to examine their selectivity for inducing transgene expression in DR DA neurons. We used immunostaining for TH, the rate-limiting enzyme in the synthesis of DA, to identify DA neurons. Co-localization analysis revealed that the majority of eYFP-expressing neurons across all four DR subregions were TH-immunopositive in DAT-Cre mice (eYFP+/TH+ 80.0%, n = 196/246 cells from n = 3 mice) (**Fig. 1h-j**). Conversely, the proportion of eYFP-positive cells that co-express detectable levels of TH-immunosignals was lower in TH-Cre mice (eYFP+/TH+ 72.9%, n = 207/284 cells from n = 2 mice) (**Fig. 1k-m**) and, strikingly, PITX3-Cre mice showed the lowest measure of TH and eYFP co-localization (eYFP+/TH+ 40.1%, n = 381/950 cells from n = 3 mice) (**Fig. 1n-p**). In light of the poor specificity for TH-immunopositive DR cells in PITX3-Cre mice, we conducted an analogous systematic anatomical analysis to examine transgene and TH co-localization in the VTA of PITX3-Cre mice (**Supplementary Fig. 1I-Q**). We analyzed co-localization of eYFP expression with

immunohistochemically detected TH across seven different areas of the caudal and rostral ventral midbrain and found an anatomical gradient in cell-type specificity. Specifically, co-localization was relatively high in the lateral part of the rostral and caudal VTA (> 70%, **Supplementary Fig. 1M, N**) in contrast to extremely low levels of co-localization observed in midline VTA regions of the caudal and rostral ventral midbrain, which is reminiscent of the expression pattern observed previously in the VTA of TH-Cre mice[7]. Taken together, our results suggest that SERT-Cre and DAT-Cre provide the highest level of selectivity for targeting transgenes to 5HT and DA neurons, respectively.

Genetically defined DR cell populations are arranged in a topographical pattern and differ in their projection targets

Motivated by reports of midbrain DA neurons that co-release glutamate[45–47] and GABA[48] as well as by the discovery of projection-defined subgroups of DR 5HT neurons that differ in their expression of a vesicular glutamate transporter[12], we next sought to ascertain the degree of overlap between genetically defined cell populations of the DR. To this end, we used VGluT3-Cre mice[49], which express Cre recombinase under control of the vesicular glutamate transporter gene *Slc17a8*, and GAD2-Cre mice[50], which express Cre recombinase under control of the glutamic acid decarboxylase 2 gene involved in GABA biosynthesis, to target DR glutamate and GABA neurons, respectively. We injected AAV-DIO-eYFP (0.3 µl) into the DR of VGluT3-Cre (**Fig. 2a**) or GAD2-Cre (**Fig. 2g, j**) mice and assayed the co-localization of eYFP with TH- and TpH-immunopositive neurons. This analysis revealed that only a very small proportion of VGluT3-expressing neurons contained TH (eYFP+/TH+ 0.4%, n = 7/1791 cells from n = 3 mice) indicating that the glutamatergic and dopaminergic DR cell populations are distinct (**Fig. 2b-d**). Conversely, there was substantial overlap of eYFP-positive/VGluT3-expressing cells with TpH, and the anatomical distribution of these doubly-labeled neurons was strongly biased in favor of the ventral DR. Specifically, 45.8% of eYFP+ cells co-expressed TpH in the ventral DR (subregion #4, eYFP+/TpH+ 45.8 %, n = 323/705 cells from n = 3 mice) compared to just 14.3% of eYFP+ cells in the dorsal DR (subregion #3, eYFP+/TpH+ 14.3%, n = 81/566 cells from n = 3), and < 5% of eYFP+ cells in each lateral subregion (subregion #1, eYFP+/TpH+ 2.1%, n = 6/292 cells; subregion #2, eYFP+/TpH+ 4.4%, n = 14/316 cells) of the DR. When the four DR subregions were considered collectively, 22.6% of all eYFP+/VGluT3-expressing cells co-expressed TpH (n = 424/1879 cells from n = 3 mice; **Fig. 2f**) and out of all eYFP+/TpH+ cells counted, a vast majority were located in the ventral DR (76.2%, n = 323/424 cells from n = 3 mice). These

data suggest that VGluT3+ neurons in the DR are subdivided into two anatomically segregated subpopulations: a dorsal group of mostly glutamate-only neurons, and a ventral group where approximately half of glutamatergic cells are also putatively serotonergic. Conversely, immunohistochemical analysis of GAD2-Cre mice revealed that eYFP-positive (i.e., GAD2-expressing) neurons are an independent cell population in the DR. Only a very small proportion of these cells contained detectable levels of TH (eYFP+/TH+ 1.4%, n = 17/1209 cells from n = 3 mice) (**Fig. 2h, i**) or TpH (eYFP+/TpH+ 0.1%, n = 2/1548 cells from n = 3 mice) (**Fig. 2k, l**). Strikingly, comparing injection sites across SERT-, ePET-, VGluT3-, GAD2-, and DAT- Cre mice revealed that genetically defined DR cell populations are arranged in a stereotyped topographical pattern that was consistent between all animals of each genotype studied (**Fig. 3, Supplementary Fig. 2**). Thus, we conclude that the DR is composed of at least five genetically defined, neurochemically distinct, and partially anatomically segregated cell types: 5HT (SERT/ePET-positive) neurons distributed all throughout the DR, GABA (GAD2-positive) neurons in the lateral DR, DA (DAT-positive) neurons in close proximity to the cerebral aqueduct, and glutamate (VGluT3-positive) neurons concentrated in the medial DR and subdivided into dorsal and ventral subpopulations with minimal and significant co-expression of 5HT cell markers, respectively (**Fig. 3, Supplementary Fig. 2**).

Next, we determined the projection targets of genetically-defined DR cell populations using six transgenic mouse lines and sampled eight brain regions previously reported to be strongly innervated by the DR[51]: the VTA, lateral hypothalamus (LH), lateral habenula (LHb), amygdala (Amy), bed nucleus of the stria terminalis (BNST), septum (SEPT), nucleus accumbens (NAc), prefrontal cortex (PFC) (**Fig. 3**). When we analyzed the projection patterns of ePET-Cre and SERT-Cre mice that received DR-targeted injections of AAV-DIO-eYFP, we found that both mouse lines display a qualitatively similar pattern across these regions with substantial eYFP terminal expression in the VTA, Amy and ventral NAc. Quantitively, however, more axon fibers were observed in these target regions in SERT-Cre mice, which is consistent with the greater penetrance for 5HT neurons observed in this mouse line. Moreover, weaker expression was observed in the LH, BNST and PFC, and very weak expression in the LHb and Sept. In VGluT3-Cre mice, we detected substantial terminal eYFP expression in the VTA and Amy, and weak expression in the LH, LHb, BNST, ventral NAc and Sept. For GAD2-Cre mice, we detected strong terminal eYFP expression in the VTA, Amy and BNST, and weaker expression in the LH, LHb and Sept. For both DAT-Cre and PITX3-Cre mice we found substantial terminal eYFP expression in the Amy, while notable

qualitative differences were observed in the LHb, and SEPT with strong labeling in PITX3-Cre mice and weak, if any, terminal eYFP expression in DAT-Cre mice. Importantly, detailed analysis of DR axon terminals in the Amy revealed divergent projection patterns that distribute putatively GABAergic input to the medial division of the central amygdala (CeA), DAergic input to the lateral division of the CeA, and glutamatergic and dopaminergic input to the capsular part of the CeA (**Fig. 3, Supplementary Fig. 3**). Together, these results suggest that (i) genetically defined 5HT, DA, GABA, and glutamate DR neuron populations are arranged in a topographical pattern that includes two anatomically distinct glutamatergic subpopulations: one with minimal, and one with significant co-expression of 5HT cell markers, (ii) DR cell populations send both convergent projections (e.g., to the LH, VTA) and divergent projections (to Amy subnuclei), and (iii) axon terminal labeling can differ quantitatively (ePET-Cre vs. SERT-Cre mice) and qualitatively (PITX3-Cre vs. DAT-Cre mice) between different Cre-driver lines intended to target the same cell populations.

Tracing monosynaptic inputs onto DR 5HT and DA neurons

Given that genetically defined DR 5HT and DA neurons differed in the locations of their cell bodies and projection targets, we next sought to identify the presynaptic partners of these cell populations. Furthermore, because targeting these cell populations with different transgenic mouse lines gave different results in our previous experiments, we hypothesized that the anatomical organization of monosynaptic inputs to DR neurons would depend not only on their neurochemical identity, but also on the specific Cre-driver lines used. To test this hypothesis, we combined a rabies virus-based genetic mapping strategy with custom semi-automated whole-brain mapping software[52]. Specifically, DAT-Cre, PITX3-Cre, SERT-Cre and ePET-Cre mice were injected with AAV-FLEX-TVA-mCherry (i.e., a cellular receptor for subgroup A avian leukosis viruses) and AAV-FLEX-RG (i.e., rabies virus glycoprotein) into the DR, followed three weeks later by RV-EnvA-ΔG-GFP (i.e., pseudotyped, glycoprotein deficient, GFP expressing rabies virus; n = 3-4 animals per mouse line) (**Fig. 4a, b**). Analysis of the starter cell populations (i.e., GFP and TVA-positive cells) in the DR of DAT-Cre mice showed that the majority of starter cells are TH-immunopositive (82.5% TH+), whereas in PITX3-Cre mice most starter cells are TH-immunonegative (77.9% TH-) (**Fig. 4c**). Conversely, the proportion of starter cells that are TpH-positive was similar between SERT-Cre and ePET-Cre mice (83.1% and 70.3%, respectively) (**Fig. 4d**). These measures of cell-type specificity in transgene (AAV-DIO-TVA-mCherry) expression were slightly lower than those observed in our Cre-line characterization experiments carried out

using AAV-DIO-eYFP likely due to the previously documented, extreme sensitivity of the pseudotyped RV toolkit to trace, background levels of TVA receptor expression in Cre-negative neurons[53]. However the trends in cell-type specificity (ePET-Cre ≈ SERT-Cre; DAT-Cre > PITX3-Cre) were consistent with our previous results, and control rabies tracing experiments in wildtype mice (C57Bl/6; n = 3 mice) and in SERT-Cre mice injected with RV-EvnA-ΔG-GFP but not FLEX-TVA or FLEX-RG (n = 3 mice) yielded very few (< 10 cells per animal) GFP-positive cells in the DR (**Supplementary Fig. 4**).

Overall, whole-brain semi-automated mapping revealed that DR 5HT neurons targeted by the SERT- and ePET-Cre lines receive nearly identical presynaptic inputs. This is consistent with results expected from monosynaptic tracing results from the same cell population accessed via two mouse lines with comparable cell-type specificities. Moreover, because RV tracing results for each input region are reported as percentages normalized to the total inputs in a given brain in order to account for stochastic differences in viral spread, differences in penetrance for 5HT neurons between the two mouse lines were also controlled for in this experiment. By contrast, DR DA neurons targeted using DAT-Cre mice receive a greater proportion of their input from anterior brain regions like as the NAc compared to DR DA neurons targeted using the PITX3-Cre mice, which receive a greater proportion of input from posterior brain areas such as the parabrachial nucleus (**Fig. 4e, f**). Thus, our results indicate that targeting the same cell population of DR DA neurons with different transgenic mouse lines can lead to anatomical differences in the neural circuits accessed at the level projection targets, cell bodies, and monosynaptic inputs.

Moreover, given that the monosynaptic inputs onto DR DA neurons have not previously been described and in light of a recent surge in interest in the organization and function of these neurons, we then compared the presynaptic partners of DR 5HT and DA neurons. We did this by pooling data from the similarly cell-type specific ePET- and SERT-Cre mice and comparing their inputs to those of DAT-Cre mice chosen for their superior cell-type specificity compared to other DA-targeting lines. In agreement with previous work, we found that major inputs onto DR 5HT neurons come from the PAG, deep mesencephalic nucleus (also known as the midbrain reticular nucleus), pontine reticular nucleus, and lateral hypothalamus[27–29]. While DR DA neurons receive input from qualitatively similar brain regions, DR DA neurons receive quantitatively more input from anterior brain regions such as the nucleus accumbens (NAc) and septum, while DR 5HT neurons receive a greater proportion of inputs from posterior brain areas like the pedunculopontine tegmentum and pontine reticular nucleus (**Fig. 5a**). Overall, DR DA neurons appeared to select a greater

proportion of their inputs from anterior brain areas compared to DR 5HT neurons (**Fig. 5a**, inset) and these differences in their inputs were sufficient to yield good separation between DA and 5HT groups via principal components analysis (**Fig. 5b**). Thus, both neurochemical identity and the specific Cre driver line used to access them are critical components that define the circuit architecture of DR neurons targeted using viral vector strategies.

Optogenetic dissection of the DR/PAG→CeA pathway

It has been suggested that DR/PAG DA neurons send dense projections to the CeA that may co-release glutamate and DA[35,37]. Specifically, using TH-Cre mice, Groessl et al.[37] demonstrated that optogenetic activation of the DR/PAG→CeA pathway induced excitatory postsynaptic currents (EPSCs) in CeA neurons presumably via synaptically released glutamate. We decided to re-evaluate these findings in light of the pronounced non-DA specific expression patterns we observed in the VTA[7] and DR (**Fig. 1k-m**) of TH-Cre mice. Because VGluT3 is selectively expressed in the DR[54], but DR DA neurons do not express VGluT3 (**Fig. 2c, d**), we hypothesized that DA and glutamate co-release in the CeA originates from VGluT2-expressing DA neurons in the nearby PAG. Alternatively, it is also possible that through the use of TH-Cre mice in which Cre expression extends beyond the targeted DA cell population, the optogenetic manipulation of unintentionally targeted glutamate cells in the DR and/or PAG could have been erroneously interpreted as dopamine and glutamate co-release. This issue is particularly important in the PAG and DR, which contain heterogeneous populations of glutamate (VGluT2- and VGluT3-expressing, respectively) neurons.

To examine the precise cellular identity and anatomical distribution of CeA-projecting neurons in the DR and PAG, we injected VGluT2-Cre mice (n = 2 mice) with fluorescent retrobeads into the CeA and AAV-DIO-eYFP (300 nl) into the DR/PAG complex (**Fig. 6a**). We found that overall in the DR and PAG 79% of the retrogradely labeled (i.e., bead-containing) neurons were TH-immunonegative (n = 94 cells), while 21% were TH-positive (n = 25 cells) confirming the presence of a dopaminergic projection in addition to projections from non-DA cell populations. Moreover, we found n = 70 bead-containing cells in the DR/PAG that co-expressed eYFP (i.e., VGluT2-expressing), but only 30% of these cells were TH-immunopositive (**Fig. 6b**, top). Strikingly, we also observed retrogradely labeled and eYFP-positive neurons in the neighboring caudal linear nucleus (CLi) and the proportion of TH-positive cells was much larger in this nucleus (72.7%) (**Fig. 6b**, bottom). Thus, CeA-

projecting neurons are located in the DR, PAG and CLi, but across these three areas only ~36% co-expressed VGluT2 and TH (**Fig. 6c**).

Next, we injected Cre-dependent AAV expressing channelrhodopsin-2 (AAV-DIO-ChR2, 300 nl) into the DR/PAG complex of VGluT2-Cre, TH-Cre (stock no. 008601, Jackson Laboratory) or DAT-Cre mice (**Fig. 6d**). Whole-cell recordings from CeA neurons revealed that light pulses that selectively stimulated VGluT2 ChR2 fibers in the CeA evoked robust EPSCs in ~59% of the recorded neurons (68.6 ± 12.1 pA, n = 17/29 cells) that were blocked by an AMPA (α-amino-3-hydroxy-5-methyl-4-isoxazole propionic acid) receptor antagonist (CNQX: 3.8 ± 1.1 pA, n = 6 cells), thus revealing a strong direct excitatory input to the CeA (**Fig. 6e)**. Importantly, while light stimulation of TH-Cre ChR2 fibers in the CeA evoked EPSCs in ~44% of the recorded CeA neurons (41.3 ± 19.3 pA, n = 11/27 cells; **Fig. 6f**), light pulses almost never evoked detectable EPSCs in CeA neurons recorded from DAT-Cre mice. Only two out of 28 recorded cells responded to light stimulation and these EPSCs had very small amplitudes (9.0 ± 1.1 pA, n = 2/28 cells; **Fig. 6g**). Thus, in light of the prominent non-DA specific expression of transgenes in TH-Cre mice, there is no satisfying functional evidence for co-release of DA and glutamate in CeA-projecting DR/PAG neurons.

DISCUSSION

Anatomical differences based on divergent transgene expression in Cre-driver lines

We have carried out a systematic, comparative evaluation of five Cre-driver mouse lines used to target the major neuromodulatory populations of the DR. In these analyses, we defined DA and 5HT neurons exclusively based on the presence of immunohistochemically detected TH or TpH proteins respectively. While we recognize that these are not perfect markers of a cell's neurochemical identity, and that subtypes of neuromodulatory neurons may be best defined using a multi-disciplinary approach integrating molecular, anatomical, and/or physiological characteristics, immunohistochemical detection of TH and TpH proteins remains the gold-standard single assay method for the identification of cells that release DA and 5HT, respectively. Thus, while TH or TpH expression does not preclude co-transmission of other neurotransmitters from these neurons, we argue that our operational definition of DA and 5HT neurons as TH+ and TpH+ cells, respectively, is appropriate for the purposes of our mouse line characterization experiments though we acknowledge that studies leveraging complementary techniques (e.g., RNA sequencing) could further contextualize these results.

Consistent with a previous study[23], we found that 5HT-targeting SERT-Cre and ePET-Cre mouse lines exhibit similar cell-type specificity. Strikingly, our data suggests that the SERT-Cre mouse line labels ~2-3 times more 5HT neurons. This trend was consistent across both the DR and MR, though we observed slightly lower cell-type specificity in the MR of ePET-Cre mice in agreement with a recent report of another transgenic mouse line based on the *PET1* gene showing reduced specificity for 5HT neurons in Brodmann's areas B8 and B9[55] corresponding to the MR[56]. The marked difference in penetrance between these two mouse lines raises the possibility that ePET-Cre mice could be labeling a defined, perhaps anatomically and/or functionally specific, subset of DR 5HT neurons that overlap partially or in whole with the set of neurons labeled by the SERT-Cre line. While further work will be necessary answer this conclusively, our experiments have shown that the ePET-Cre line labeled 5HT neurons without any obvious bias for any DR subregion and that the afferent and efferent connectivities of DR 5HT neurons targeted with the ePET-Cre and SERT-Cre mouse lines are largely similar. This argues against the idea that the ePET-Cre line is labeling an anatomically specific subset of 5HT neurons compared to the SERT-Cre line and instead suggests both lines sample different proportions of the same pool of neurons. In turn, this has important implications for the interpretation and future design of cell-type specific manipulations of 5HT neurons since it suggests that identical experiments performed in SERT-Cre and ePET-Cre mice would likely recruit different proportions of the DR or MR 5HT systems, potentially leading to divergent behavioral or physiological responses.

On the other hand, we have found dramatic differences in cell-type specificity between DAT-, TH-, and PITX3-Cre mice targeting DR DA neurons. All three lines showed appreciable levels of Cre expression in TH-immunonegative DR neurons, but our data indicate that DAT-Cre mice provide the most specific genetic handle onto this DA cell population. The reduced cell-type specificity we described in the TH- and PITX3-Cre mouse lines relative to the DAT-Cre line could theoretically be explained by some Cre+ neurons expressing low levels of TH-protein below the immunodetection limit or by limitations associated with our immunostaining or imaging procedures. However, this is unlikely to account for the labeling we observed for a few reasons. First, the qualitative observation of Cre+/TH- neurons in the PITX3- and TH-Cre mouse lines has also been made by others using different staining reagents and imaging strategies[43,44,57]. Second, the distribution of eYFP+/TH- cells near the DR in TH-Cre and PITX3-Cre mice extended into the lateral PAG and DpME regions (i.e. midbrain reticular nucleus) where very few and no DA neurons are known to reside, respectively, and this was not observed in the more cell-type specific DAT-

Cre line. Third, the distribution of Cre+ cells in the midbrain of TH-Cre and PITX3-Cre mice extended into VTA regions not known to contain any DA neurons (e.g., interpeduncular nucleus (IPN))[7]. Together, these lines of evidence support the interpretation that the TH-Cre and PITX3-Cre mouse lines exhibit prominent Cre expression in TH-immunonegative neurons of the VTA and DR. As has been discussed previously[7], this finding informs the interpretation of supposedly DA-specific manipulations which in the case of the TH- and PITX3-Cre lines are likely recruiting non-DA neurons.

Remarkably, the non-DA neuron labeling pattern observed in the medial ventral midbrain of PITX3-Cre mice was strikingly similar to that observed in TH-Cre mice[7]. While the PITX3-Cre line tended to label fewer neurons in the IPN, both lines showed prominent Cre expression in the interfascicular nucleus and rostral linear nucleus (RLi). The finding that these neurons are labeled by mouse lines under the control of genes expressed early (TH, PITX3), but not later in the development of the mesencephalon (DAT), suggests that some of these eYFP+/TH- neurons may have transiently expressed DA-related genes at some stage in their development but subsequently lost the ability to synthesize DA[43], which is sometimes referred to as 'ectopic expression'[58]. Thus, it is possible that in adult TH-Cre and PITX3-Cre mice, Cre-recombinase is present in cells that do not contain TH mRNA at all. Such Cre-expressing cells have been found in the RLi of PITX3-Cre mice[44]. Moreover, other Cre-positive cells express TH mRNA, but may not translate it into proteins. Such cells have been found in the IPN of TH-Cre mice[7]. Importantly, while Cre-expressing RLi and IPN neurons lack the molecular machinery to produce DA, RLi neurons express VGluT2 suggesting that these cells could be functionally glutamatergic[44]. It is essential to detect and examine these unwanted recombination events as they may have implications for the interpretation of neural circuit structure and function.

In addition to differences in the distribution of Cre+ cell bodies between the mouse lines described above, the neural circuits accessed via different mouse lines targeting DR neuromodulatory systems also differed with respect to their afferent and efferent connections. DR 5HT neurons accessed via the SERT-Cre and ePET-Cre mouse lines displayed qualitatively similar axon distribution patterns in eight known DR 5HT projection target regions. However, quantitatively more fiber labeling was observed in SERT-Cre mice which is consistent with their greater penetrance for 5HT neurons. On the other hand, projection patterns differed qualitatively between the DAT-Cre and PITX3-Cre mouse lines targeting DR DA neurons, with the PITX3-Cre line showing projections to the SEPT and LHb, where very few if any terminals could be seen in DAT-Cre mice. This suggests that projections from

the DR to the SEPT and LHb originate largely from TH-immunonegative (non-DA) DR neurons that are labeled in the non-cell-type-specific PITX3-Cre mouse line. Monosynaptic rabies tracing analyses revealed DR 5HT neurons accessed with the SERT-Cre and ePET-Cre mouse lines sample a nearly identical distribution of inputs, while DR DA neurons targeted with the DAT-Cre and PITX3-Cre mouse lines received a different proportion of their inputs from striatum and SEPT. These results indicate that the choice of Cre-drive mouse line used to access neuromodulatory populations leads to systematic anatomical differences in the neural circuits accessed.

Functional differences based on divergent transgene expression in Cre-driver lines

Using TH-Cre mice, a recent study suggested that DR/PAG DA neurons co-release DA and glutamate, which may directly reinforce fear learning in the CeA circuitry in response to aversive stimuli[37]. Although there is evidence that DR/PAG terminals release DA in the CeA *in vivo*[35], our data argues against the possibility that glutamate and DA is co-released from the same cell population. We found that the majority (~70%) of DR/PAG neurons projecting to the CeA are glutamatergic (i.e., VGluT2-positive) and these cells not co-express detectable levels of TH proteins. While TH-immunopositive neurons labeled by VGluT2 reporter lines have been described previously in the DR/PAG[34,35], our data suggests that TH protein is expressed in only ~30% of CeA-projecting DR/PAG neurons. Importantly, we were not able to reliably detect EPSCs in CeA neurons when stimulating DR/PAG terminals in DAT-Cre mice suggesting that even though a few DR/PAG TH-positive cells co-express VGluT2 there is no satisfying functional evidence for DA and glutamate co-release in this pathway. Only 2 out of 28 recorded cells displayed very small EPSCs (<10 pA) and these may have been very well within noise levels. In light of the prominent non-DA specific expression patterns observed in TH-Cre mice and the fact that we were able to detect light-evoked EPSCs in CeA neurons recorded in TH-Cre, but not DAT-Cre mice, we conclude that it is unlikely that CeA-projecting DR/PAG neurons co-release DA and glutamate. We argue that DA and glutamate are released from separate populations of DR/PAG neurons and that the EPSCs recorded in CeA neurons from TH-Cre mice are more likely attributed to the unintentional expression of ChR2 in DR/PAG glutamate neurons. Nonetheless, the possibility of DA and co-release in the CeA cannot be excluded entirely as another study was able to detected light evoked EPSCs in CeA neurons in response to optogenetic stimulation of DR terminals in DAT-Cre mice[35]. Considering that the proportion of CeA-projecting cells that co-express VGluT2 and TH is greater in the CLi, it is conceivable that sufficient virus leaking into the CLi may

produce EPSCs even in DAT-Cre mice. Thus, while there is evidence that some DA neurons may co-release glutamate[45–47] or GABA[48], additional studies examining this phenomenon in the DR/PAG are necessary.

Implications for experimental design using Cre-driver mouse lines to access DA and 5HT neurons

Based on these results, we suggest that researchers make the following considerations when designing experiments that involve transgenic animals. First, our results illustrate the advantages of using a comparative, systematic approach for evaluating the strengths and caveats associated with a given mouse line. This is because without comparing the SERT-Cre and ePET-Cre mice side-by-side, we would have concluded that each mouse line individually shows high cell-type specificity for 5HT neurons without identifying potential differences between them relevant to experimental design, such as the superior penetrance of the SERT-Cre line. Similarly, a qualitative evaluation confirming the existence VGlut3/TpH co-expressing neurons in the DR would not have detected the dorsal-to-ventral gradient in coexpression revealed by our quantitative analysis. Thus, it is important to deliberately determine the extent and distribution of recombination events in each mouse line to avoid misinterpretations of results from animals with patterns of Cre expression that are not fully characterized[58]. These characterization experiments are particularly important in light of documented instances of Cre expression has extending beyond the targeted cell population despite faithfully recapitulating the endogenous expression pattern of its promoting gene (e.g., Cre expression in IPN neurons that express TH mRNA but not TH protein)[7].

Secondly, even though our data suggest that the TH-Cre and PITX3-Cre mouse lines may not be suitable for cell-type specific manipulations of DR DA neurons, this should not imply that these lines are not useful for other applications, for example when combined with complementary methodologies (e.g, pharmacological manipulations). As such, the TH-Cre mouse line labels mesocortical VTA DA neurons, which are likely to be undersampled by the DAT-Cre mouse line[59,60]. Furthermore, the PITX3-Cre and ePET-Cre mouse lines label DA or 5HT neurons, respectively, at a much earlier developmental time point compared to the DAT-Cre and SERT-Cre lines[44,61]. Despite the reduced cell-type specificity or penetrance of these lines then, they continue to be the most appropriate tools for studying the early assembly of these neuromodulatory circuits and integrating the use of these mouse lines with complementary approaches (e.g. intersectional targeting with flp-recombinase driver lines or viral vectors) may help to overcome some the caveats associated with them. Thus, we

interpret our results as evidence in favor of the establishment of a case-by-case framework for the evaluation of suitability of each transgenic mouse line for accomplishing a specific scientific goal.

Thirdly, it is critical to control for potential caveats associated with the use of Cre-driver lines. For example, the cell-type specificity of a given mouse line can differ between nearby brain regions (e.g., lateral to medial gradient in cell-type specificity of PITX3-Cre and TH-Cre mice). This suggests the need to analyze and document transgene expression beyond the intended viral injection site for individual animals. While canula or optical fiber placements are often histologically verified and reported, detailed characterization of viral spread in each animal is much less common.

Refined model of DR circuitry and conclusions

Using these characterized mouse lines, we have shown that genetically defined DR 5HT, DA, GABA and glutamate populations are arranged in a topographical pattern, and that with the exception of putatively glutamate and 5HT co-transmitting (i.e. VgluT3+/TpH+) neurons, these populations are largely distinct from each other. This result is in agreement with a previous report describing the nearly complementary distribution patterns of DR glutamate and GABA neurons in the rat[23,62], and with previous observations of the lateral distribution of DR GABA cells in mice[23,25,29,63]. Furthermore, other reports have also shown that VGluT3+/TpH+ doubly labeled neurons are predominantly found in the ventral dorsal raphe in rats[62], and that cortically-projecting 5HT neurons in the ventral DR of mice co-express VGluT3[12]. Nonetheless, our description of organization of the DR includes all four major cell types along with a detailed quantitative analysis of their distribution and overlap. In addition, we performed a comparative analysis of the projections from all four major DR cell types eight brain areas known to be innervated by the DR and the first description of monosynaptic inputs onto DR DA neurons. Thus, our results provide the anatomical basis for future cell-type and projection-specific functional investigations into the DR circuitry, and furthermore illustrate how the systematic evaluation and application of Cre-driver mouse lines advances our understanding of the anatomical and functional diversity of heterogeneous brain regions.

METHODS

Subjects. The following mouse lines (25-30 g, 8-14 weeks old, male) were used for experiments: C57BL/6 mice (Jackson Laboratory), DAT::IRES-Cre (Jackson Laboratory,

stock number: *006660*, strain code: B6.SJL-Slc6a3tm1.1(cre)Bkmn/J), VGLUT2::IRES-Cre (Jackson Laboratory, stock number: *016963*, strain code: Slc17a6tm2(cre)Lowl/J), GAD2::IRES-Cre (Jackson Laboratory, stock number: *010802*, strain code: Gad2$^{tm2(cre)Zjh}$/J), VGLUT3-Cre (Jackson Laboratory, stock number: 018147, strain code: Tg(Slc17a8-icre)1Edw/SealJ), TH-Cre (Jackson Laboratory, stock number: 008601, strain code: B6.Cg-Tg(Th-cre)1Tmd/J), SERT-Cre (Mouse Mutant Resource and Research Centers, stock number: 017260-UCD, strain code: Tg(Slc6a4-cre)ET33Gsat/Mmucd), ePET-Cre (Jackson Laboratory, stock number: 012712, strain code: B6.Cg-Tg(Fev-cre)1Esd/J) and PITX3-Cre[43]. All lines have been crossed onto the C57BL/6 background for at least 6 generations. Mice were maintained on a 12:12 light cycle (lights on at 07:00). All procedures complied with the animal care standards set forth by the National Institutes of Health and were approved by University of California, Berkeley's Administrative Panel on Laboratory Animal Care.

Stereotaxic Injections. As previously described[7] all stereotaxic injections were performed under general ketamine–dexmedetomidine anesthesia using a stereotaxic instrument (Kopf Instruments, Model 1900). For red fluorescent retrobead labeling, mice were injected unilaterally with fluorescent retrobeads (100 nl; LumaFluor Inc.) in the central nucleus of the amygdala (CeA; bregma: -1.22 mm, lateral: 2.8 mm, ventral: -4.7 mm) using a 1 µl Hamilton syringe (Hamilton). The AAVs (adeno associated virus) used in this study were from the Deisseroth laboratory (AAV5-EF1α–DIO-hChR2(H134R)-eYFP, AAV5-EF1α-DIO-eYFP; ~10^{12} infectious units per ml, prepared by the University of North Carolina Vector Core Facility) or from the Uchida laboratory (AAV5-flex-RG; AAV5-flex-TVA-mCherry; ~10^{12} infectious units per ml, prepared by the University of North Carolina Vector Core Facility). RV-EnvA-ΔG-GFP was prepared by Kevin Beier. For viral injections, 0.3-1 µl of concentrated virus solution was injected unilaterally into the DR/PAG (bregma: -4.36 mm, lateral: 0 mm, ventral: -3.2 mm), MnR (bregma: -4.36 mm, lateral: 0 mm, ventral: -4.4 mm) or VTA (bregma: -3.4 mm, lateral: 0.3 mm, ventral: -4.4 mm) using a syringe pump (Harvard Apparatus) at 150 nl/min. The injection needle was withdrawn 5 min after the end of the infusion. The animal was kept on a heating pad until it recovered from anesthesia. Experiments were performed 4-6 weeks (for AAVs) or 7 days (for retrobeads) after stereotactic injection. Injection sites were confirmed in all animals by preparing coronal sections (50 or 100 µm).

Transsynaptic Rabies Virus Tracing. We used a rabies virus-based genetic mapping strategy [64] to label presynaptic inputs onto designated starter cell populations, and quantified input cell data using a semi-automated whole-brain mapping MATLAB scripts[52]. Specifically, DAT-Cre, PITX3-Cre, SERT-Cre and ePET-Cre mice were injected with AAV-FLEX-TVA (i.e., a cellular receptor for subgroup A avian leukosis viruses) and AAV-FLEX-RG (i.e., rabies virus glycoprotein) (800 nl, 1:1) into the DR and four weeks later, 300 nl RV-EnvA-ΔG-GFP (i.e., pseudotyped, glycoprotein deficient, GFP expressing rabies virus) was injected into the same region (see "Stereotaxic Injections" for coordinates). Seven days after injection, mice were perfused with 4% paraformaldehyde (PFA) in PBS. For input mapping, 75 µm sections of the whole brain were prepared and scanned using a Zeiss Axio Scan Z1. Individual slices were aligned using customized Matlab scripts. GFP-positive pixels were identified on the basis of a pixel-intensity threshold in the green channel. False-positive pixels (artefacts) were manually identified and removed. Positive pixels were assigned to different brain areas based on "*The Mouse Brain in Stereotaxic Coordinates*"[56] (**Fig. 4a**). Pixels per brain area were then represented as a percentage of total input pixels. Twelve brain regions were randomly selected to validate this method and a human observer counted GFP-positive cells in these regions. These results demonstrated a high correlation between manually scoring of input neurons by an independent observer and our automated segmentation procedure (**Fig. 4b**; $R^2 = 0.9434$, n = 12 brain regions).

Electrophysiology. Mice were deeply anaesthetized with pentobarbital (200 mg/kg ip; Vortech). Coronal midbrain slices (200 µm) were prepared after intracardial perfusion with ice-cold artificial cerebrospinal fluid (ACSF) containing (in mM) 50 sucrose, 125 NaCl, 25 $NaHCO_3$, 2.5 KCl, 1.25 NaH_2PO_4, 0.1 $CaCl_2$, 4.9 $MgCl_2$, and 2.5 glucose (oxygenated with 95% O_2/5% CO_2). After 90 min of recovery, slices were transferred to a recording chamber and perfused continuously at 2-4 ml/min with oxygenated ACSF, containing (in mM) 125 NaCl, 25 $NaHCO_3$, 2.5 KCl, 1.25 NaH_2PO_4, 11 glucose, 1.3 $MgCl_2$ and 2.5 $CaCl_2$ at ~30 ºC. For recording of excitatory postsynaptic currents (EPSCs) picrotoxin (50 µM, Sigma) was added to block inhibitory currents mediated by $GABA_A$ receptors. Cells were visualized with a 40x water-immersion objective on an upright fluorescent microscope (BX51WI; Olympus) equipped with infrared-differential interference contrast video microscopy and epifluorescence (Olympus). Patch pipettes (3.8-4.4 MΩ) were pulled from borosilicate glass (G150TF-4; Warner Instruments) and filled with internal solution, which consisted of (in mM) 117 $CsCH_3SO_3$, 20 HEPES, 0.4 EGTA, 2.8 NaCl, 5 TEA, 4 MgATP, 0.3 NaGTP, 5

QX314 and 0.1% neurobiotin, pH 7.35 (270–285 mOsm). Electrophysiological recordings were made using a MultiClamp700B amplifier and acquired using a Digidata 1550 digitizer, sampled at 10 kHz, and filtered at 2 kHz. All data acquisition was performed using pCLAMP software (Molecular Devices). Channelrhodopsin-2 (ChR2) was stimulated by flashing 473 nm light through the light path of the microscope using an ultrahigh-powered light-emitting diode (LED) powered by an LED driver (Prizmatix) under computer control. A dual lamp house adaptor (Olympus) was used to switch between fluorescence lamp and LED light source. The light intensity of the LED was not changed during the experiments and the whole slice was illuminated (5 mW/mm^2). Light-evoked excitatory postsynaptic currents (EPSCs) were obtained every 10 s with one pulse of 473 nm light (5 ms) with neurons voltage clamped at -70 mV. Series resistance (15–25 MΩ) and input resistance were monitored online. For pharmacological experiments, we recorded baseline responses for 3 min and bath applied 10 μM CNQX (Tocris) for 5-10 min to block AMPA/kainate receptor mediated currents. Data were analyzed offline using IgorPro Software (Wavemetrics). Light-evoked EPSC amplitudes were calculated by averaging responses from 10 sweeps and then measuring the peak amplitude in a 50 ms window after the light pulse. Cells that did not show a peak in this window that exceeded the baseline noise were classified as non-responders.

Histology, Immunofluorescence, and Confocal Microscopy. Immunohistochemistry and confocal microscopy were performed as described previously[7]. Briefly, after intracardial perfusion with 4% PFA in PBS, pH 7.4, the brains were post-fixed overnight and coronal brain slices (50, 75 or 100 μm) were prepared. The primary antibodies used were rabbit anti-tyrosine hydroxylase (TH) (1:1000, Millipore), mouse anti-TH (1:1000, Millipore), and rabbit anti-tryptophan hydroxylase 2 (TpH) (1:1000, Millipore). The secondary antibodies used were AlexaFluor546 goat anti-rabbit and Alexa Fluor647 goat anti-mouse (all 1:750, Molecular Probes). Image acquisition was performed with Zeiss LSM510 and LSM710 laser scanning confocal microscope using 10x and 40x objectives and on a Zeiss AxioImager M2 upright widefield fluorescence/differential interference contrast microscope with charge-coupled device camera using a 5x objective. Confocal images were analyzed using ImageJ and the Zeiss LSM Image Browser software.

For anatomical characterization and quantification of eYFP-expressing neurons in the VTA, DR and MnR using different transgenic mouse lines, 50 μm coronal sections of the brain area of interest were collected (VTA; bregma: -2.92 to -3.88 mm; DR, bregma: -4.24 to -4.96 mm; MnR, bregma: -4.04 to -4.96 mm) and every other section was analyzed. In every

section analyzed, the DR was divided into four subregions measuring ~300 x 300 µm and one confocal image covering 230 x 230 µm was acquired in each subregion that contained at least one eYFP+ cell. Confocal images were non-overlapping and were acquired using identical pinhole and laser settings. All sections were labelled relative to bregma using landmarks and neuroanatomical nomenclature as described in "*The Mouse Brain in Stereotaxic Coordinates*" [56]. The total number of eYFP-expressing TpH-immunopositive and TpH-immunonegative, or eYFP-expressing TH-immunopositive, and TH-immunonegative, neurons was calculated for each of the four subregions. The same methodological approach was used for quantification of retrogradely labeled (i.e. bead-containing) neurons in the DR/PAG complex (**Fig. 6**). However, in addition to the retrogradely labeled neurons in the DR, bead-containing neurons in the PAG (bregma: bregma: -4.04 to 4.24 mm) and caudal linear nucleus (CLi, bregma: -4.04 to 4.24 mm) were analyzed. The anatomical characterization and quantification of eYFP-expressing neurons in the VTA using PITX3-Cre mice (**Supplementary Fig. 1**), was performed according to the procedures and anatomical landmarks described in Lammel et al., 2015[7].

Statistics. Student's paired and unpaired t tests were used to determine statistical differences for anatomical and electrophysiological data using GraphPad Prism 6 (Graphpad Software). Statistical significance was * $p < 0.05$, ** $p < 0.01$, *** $p < 0.001$. All data are presented as means ± SEM.

Code availability. All custom code used for analysis in this manuscript is available on request.

REFERENCES

1. Cardozo Pinto, D. F. & Lammel, S. Viral vector strategies for investigating midbrain dopamine circuits underlying motivated behaviors. *Pharmacol. Biochem. Behav.* **174**, 23–32 (2018).
2. Deisseroth, K. & Schnitzer, M. J. Engineering Approaches to Illuminating Brain Structure and Dynamics. *Neuron* **80**, 568–577 (2013).
3. Gong, S. *et al.* Targeting Cre recombinase to specific neuron populations with bacterial artificial chromosome constructs. *J. Neurosci. Off. J. Soc. Neurosci.* **27**, 9817–9823 (2007).
4. Luo, L., Callaway, E. M. & Svoboda, K. Genetic Dissection of Neural Circuits: A Decade of Progress. *Neuron* **98**, 256–281 (2018).
5. Schwarz, L. A. *et al.* Viral-genetic tracing of the input-output organization of a central noradrenaline circuit. *Nature* **524**, 88–92 (2015).

6. Zhuang, X., Masson, J., Gingrich, J. A., Rayport, S. & Hen, R. Targeted gene expression in dopamine and serotonin neurons of the mouse brain. *J. Neurosci. Methods* **143**, 27–32 (2005).
7. Lammel, S. *et al.* Diversity of transgenic mouse models for selective targeting of midbrain dopamine neurons. *Neuron* **85**, 429–438 (2015).
8. Stuber, G. D., Stamatakis, A. M. & Kantak, P. A. Considerations When Using Cre-Driver Rodent Lines for Studying Ventral Tegmental Area Circuitry. *Neuron* **85**, 439–445 (2015).
9. Hainer, C. *et al.* Beyond Gene Inactivation: Evolution of Tools for Analysis of Serotonergic Circuitry. *ACS Chem. Neurosci.* **6**, 1116–1129 (2015).
10. Scott, M. M. *et al.* A genetic approach to access serotonin neurons for in vivo and in vitro studies. *Proc. Natl. Acad. Sci.* **102**, 16472–16477 (2005).
11. Gagnon, D. & Parent, M. Distribution of VGLUT3 in Highly Collateralized Axons from the Rat Dorsal Raphe Nucleus as Revealed by Single-Neuron Reconstructions. *PLoS ONE* **9**, e87709 (2014).
12. Ren, J. *et al.* Anatomically Defined and Functionally Distinct Dorsal Raphe Serotonin Sub-systems. *Cell* **175**, 472-487.e20 (2018).
13. Correia, P. A., Matias, S. & Mainen, Z. F. Stereotaxic Adeno-associated Virus Injection and Cannula Implantation in the Dorsal Raphe Nucleus of Mice. *Bio-Protoc.* **7**, e2549 (2017).
14. Warden, M. R. *et al.* A prefrontal cortex-brainstem neuronal projection that controls response to behavioural challenge. *Nature* **492**, 428–432 (2012).
15. Li, Y. *et al.* Serotonin neurons in the dorsal raphe nucleus encode reward signals. *Nat. Commun.* **7**, (2016).
16. Liu, Z. *et al.* Dorsal Raphe Neurons Signal Reward through 5-HT and Glutamate. *Neuron* **81**, 1360–1374 (2014).
17. Zhong, W., Li, Y., Feng, Q. & Luo, M. Learning and Stress Shape the Reward Response Patterns of Serotonin Neurons. *J. Neurosci.* **37**, 8863–8875 (2017).
18. Marcinkiewcz, C. A. *et al.* Serotonin engages an anxiety and fear-promoting circuit in the extended amygdala. *Nature* **537**, 97–101 (2016).
19. Dugué, G. P. *et al.* Optogenetic Recruitment of Dorsal Raphe Serotonergic Neurons Acutely Decreases Mechanosensory Responsivity in Behaving Mice. *PLoS ONE* **9**, e105941 (2014).
20. Dölen, G., Darvishzadeh, A., Huang, K. W. & Malenka, R. C. Social reward requires coordinated activity of nucleus accumbens oxytocin and serotonin. *Nature* **501**, 179–184 (2013).
21. Walsh, J. J. *et al.* 5-HT release in nucleus accumbens rescues social deficits in mouse autism model. *Nature* **560**, 589–594 (2018).
22. Fonseca, M. S., Murakami, M. & Mainen, Z. F. Activation of Dorsal Raphe Serotonergic Neurons Promotes Waiting but Is Not Reinforcing. *Curr. Biol.* **25**, 306–315 (2015).
23. McDevitt, R. A. *et al.* Serotonergic versus Nonserotonergic Dorsal Raphe Projection Neurons: Differential Participation in Reward Circuitry. *Cell Rep.* **8**, 1857–1869 (2014).
24. Miyazaki, K. W. *et al.* Optogenetic Activation of Dorsal Raphe Serotonin Neurons Enhances Patience for Future Rewards. *Curr. Biol.* **24**, 2033–2040 (2014).
25. Seo, C. *et al.* Intense threat switches dorsal raphe serotonin neurons to a paradoxical operational mode. *Science* **363**, 538–542 (2019).
26. Cohen, J. Y., Amoroso, M. W. & Uchida, N. Serotonergic neurons signal reward and punishment on multiple timescales. *eLife* **4**, (2015).

27. Ogawa, S. K., Cohen, J. Y., Hwang, D., Uchida, N. & Watabe-Uchida, M. Organization of Monosynaptic Inputs to the Serotonin and Dopamine Neuromodulatory Systems. *Cell Rep.* **8**, 1105–1118 (2014).
28. Pollak Dorocic, I. *et al.* A Whole-Brain Atlas of Inputs to Serotonergic Neurons of the Dorsal and Median Raphe Nuclei. *Neuron* **83**, 663–678 (2014).
29. Weissbourd, B. *et al.* Presynaptic Partners of Dorsal Raphe Serotonergic and GABAergic Neurons. *Neuron* **83**, 645–662 (2014).
30. Sengupta, A., Bocchio, M., Bannerman, D. M., Sharp, T. & Capogna, M. Control of Amygdala Circuits by 5-HT Neurons via 5-HT and Glutamate Cotransmission. *J. Neurosci. Off. J. Soc. Neurosci.* **37**, 1785–1796 (2017).
31. Dougalis, A. G. *et al.* Functional properties of dopamine neurons and co-expression of vasoactive intestinal polypeptide in the dorsal raphe nucleus and ventro-lateral periaqueductal grey: DRN/vlPAG dopamine neurons. *Eur. J. Neurosci.* **36**, 3322–3332 (2012).
32. Cho, J. R. *et al.* Dorsal Raphe Dopamine Neurons Modulate Arousal and Promote Wakefulness by Salient Stimuli. *Neuron* **94**, 1205-1219.e8 (2017).
33. Hasue, R. H. & Shammah-Lagnado, S. J. Origin of the dopaminergic innervation of the central extended amygdala and accumbens shell: a combined retrograde tracing and immunohistochemical study in the rat. *J. Comp. Neurol.* **454**, 15–33 (2002).
34. Li, C. *et al.* Mu Opioid Receptor Modulation of Dopamine Neurons in the Periaqueductal Gray/Dorsal Raphe: A Role in Regulation of Pain. *Neuropsychopharmacology* **41**, 2122–2132 (2016).
35. Matthews, G. A. *et al.* Dorsal Raphe Dopamine Neurons Represent the Experience of Social Isolation. *Cell* **164**, 617–631 (2016).
36. Taylor, N. E. *et al.* The Role of Glutamatergic and Dopaminergic Neurons in the Periaqueductal Gray/Dorsal Raphe: Separating Analgesia and Anxiety. *eNeuro,* DOI: https://doi.org/10.1523/ENEURO.0018-18.2019 33 (2019).
37. Groessl, F. *et al.* Dorsal tegmental dopamine neurons gate associative learning of fear. *Nat. Neurosci.* **21**, 952–962 (2018).
38. Lammel, S., Lim, B. K. & Malenka, R. C. Reward and aversion in a heterogeneous midbrain dopamine system. *Neuropharmacology* **76 Pt B**, 351–359 (2014).
39. Morales, M. & Margolis, E. B. Ventral tegmental area: cellular heterogeneity, connectivity and behaviour. *Nat. Rev. Neurosci.* **18**, 73–85 (2017).
40. Roeper, J. Dissecting the diversity of midbrain dopamine neurons. *Trends Neurosci.* **36**, 336–342 (2013).
41. Bäckman, C. M. *et al.* Characterization of a mouse strain expressing Cre recombinase from the 3' untranslated region of the dopamine transporter locus. *Genes. N. Y. N 2000* **44**, 383–390 (2006).
42. Savitt, J. M. Bcl-x Is Required for Proper Development of the Mouse Substantia Nigra. *J. Neurosci.* **25**, 6721–6728 (2005).
43. Smidt, M. P., von Oerthel, L., Hoekstra, E. J., Schellevis, R. D. & Hoekman, M. F. M. Spatial and Temporal Lineage Analysis of a Pitx3-Driven Cre-Recombinase Knock-In Mouse Model. *PLoS ONE* **7**, e42641 (2012).
44. Tiklová, K. *et al.* Single-cell RNA sequencing reveals midbrain dopamine neuron diversity emerging during mouse brain development. *Nat. Commun.* **10**, 581 (2019).
45. Hnasko, T. S. *et al.* Vesicular glutamate transport promotes dopamine storage and glutamate corelease in vivo. *Neuron* **65**, 643–56 (2010).
46. Stuber, G. D., Hnasko, T. S., Britt, J. P., Edwards, R. H. & Bonci, A. Dopaminergic Terminals in the Nucleus Accumbens But Not the Dorsal Striatum Corelease Glutamate. *J. Neurosci.* **30**, 8229–8233 (2010).

47. Tecuapetla, F. *et al.* Glutamatergic signaling by mesolimbic dopamine neurons in the nucleus accumbens. *J Neurosci* **30**, 7105–10 (2010).
48. Tritsch, N. X., Granger, A. J. & Sabatini, B. L. Mechanisms and functions of GABA co-release. *Nat. Rev. Neurosci.* **7**, 139-45 (2016).
49. Grimes, W. N., Seal, R. P., Oesch, N., Edwards, R. H. & Diamond, J. S. Genetic targeting and physiological features of VGLUT3+ amacrine cells. *Vis. Neurosci.* **28**, 381–392 (2011).
50. Taniguchi, H. *et al.* A resource of Cre driver lines for genetic targeting of GABAergic neurons in cerebral cortex. *Neuron* **71**, 995–1013 (2011).
51. Vertes, R. P. A PHA-L analysis of ascending projections of the dorsal raphe nucleus in the rat. *J. Comp. Neurol.* **313**, 643–668 (1991).
52. de Jong, J. W. *et al.* A Neural Circuit Mechanism for Encoding Aversive Stimuli in the Mesolimbic Dopamine System. *Neuron* **101**, 133-151.e7 (2019).
53. Miyamichi, K. *et al.* Dissecting local circuits: parvalbumin interneurons underlie broad feedback control of olfactory bulb output. *Neuron* **80**, 1232–1245 (2013).
54. Wang, H. L. & Morales, M. Pedunculopontine and laterodorsal tegmental nuclei contain distinct populations of cholinergic, glutamatergic and GABAergic neurons in the rat. *Eur J Neurosci* **29**, 340–58 (2009).
55. Pelosi, B., Migliarini, S., Pacini, G., Pratelli, M. & Pasqualetti, M. Generation of Pet1210-Cre transgenic mouse line reveals non-serotonergic expression domains of Pet1 both in CNS and periphery. *PloS One* **9**, e104318 (2014).
56. Franklin, K. B. J. & Paxinos, G. *Paxinos and Franklin's The mouse brain in stereotaxic coordinates*. (Academic Press, an imprint of Elsevier, 2013).
57. Vuong, H. E., Pérez de Sevilla Müller, L., Hardi, C. N., McMahon, D. G. & Brecha, N. C. Heterogeneous transgene expression in the retinas of the TH-RFP, TH-Cre, TH-BAC-Cre and DAT-Cre mouse lines. *Neuroscience* **307**, 319–337 (2015).
58. Song, A. J. & Palmiter, R. D. Detecting and Avoiding Problems When Using the Cre–lox System. *Trends Genet.* **34**, 333–340 (2018).
59. Lammel, S. *et al.* Unique properties of mesoprefrontal neurons within a dual mesocorticolimbic dopamine system. *Neuron* **57**, 760–73 (2008).
60. Vander Weele, C. M. *et al.* Dopamine enhances signal-to-noise ratio in cortical-brainstem encoding of aversive stimuli. *Nature* **563**, 397–401 (2018).
61. Deneris, E. S. Molecular genetics of mouse serotonin neurons across the lifespan. *Neuroscience* **197**, 17–27 (2011).
62. Hioki, H. *et al.* Vesicular glutamate transporter 3-expressing nonserotonergic projection neurons constitute a subregion in the rat midbrain raphe nuclei: VGLUT3-Expressing Nonserotonergic Neurons in DR. *J. Comp. Neurol.* **518**, 668–686 (2010).
63. Nectow, A. R. *et al.* Identification of a Brainstem Circuit Controlling Feeding. *Cell* **170**, 429-442.e11 (2017).
64. Osakada, F. & Callaway, E. M. Design and generation of recombinant rabies virus vectors. *Nat. Protoc.* **8**, 1583–1601 (2013).

ACKNOWLEDGEMENTS

We are grateful to Johannes W. de Jong for the use of his custom MATLAB scripts for analyzing rabies tracing input data and to Seyedeh Atiyeh Afjei for technical assistance. We thank the entire Lammel laboratory for helpful discussion, the UNC vector core for AAV viruses and the CNR Biological Imaging Facility at the University of California, Berkeley. S.L. is a John P. Stock Faculty Fellow and Rita Allen Scholar. This work was supported by

grants from NIDA (R01-DA042889), NIMH (R01MH112721), the Rita Allen Foundation, the Wayne and Gladys Valley Foundation, a NARSAD Young Investigator Award (23543) and a Brain Research Foundation grant (BRFSG-2015-7). I.P.D. is supported by a postdoctoral fellowship from the Wenner-Gren Foundation. D.C.P. was supported by an Amgen Scholarship and a Graduate Research Fellowship from the National Science Foundation.

AUTHOR CONTRIBUTIONS

Stereotactic injections were performed by D.C.P., I.P.D., and H.Y. Immunohistochemistry and microscopy were by D.C.P. and V.J.H. Rabies tracing was by D.C.P, V.J.H., and I.P.D. Rabies virus was produced by K.T.B. Electrophysiology was by H.Y. PITX3-Cre mice were provided by M.P.S. The study was designed by D.C.P. and S.L. Results were analyzed and interpreted by D.C.P. and S.L. The manuscript was written by D.C.P. and S.L. and edited by all authors.

CONFLICT OF INTEREST STATEMENT

The authors declare no competing interests.

FIGURE LEGENDS

Figure 1. Anatomical characterization of 5HT and DA neuron-targeting transgenic mouse lines in the dorsal raphe nucleus.

(a) Schematic of experimental design showing viral injection into the DR of SERT-Cre and ePET-Cre mice (to target 5HT neurons) and of DAT-Cre, TH-Cre and PITX3-Cre mice (to target DA neurons).

(b) Confocal image showing co-localization of eYFP (green) and tryptophan hydroxylase 2 (TpH) immunopositive (red) neurons in the DR, which is subdivided into four numbered subregions (scale bar 1 mm).

(c) Confocal images showing eYFP and TpH-positive neurons for the subregions in (b). Vertical slice charts indicate percentage of eYFP-positive cells that co-express TpH (eYFP+ TpH+, blue) or lack expression of TpH (eYFP+ TpH-, orange) in individual DR subregions (scale bar 50 μm).

(d) Pie chart showing total percentage of eYFP+ and TpH+ (blue) and eYFP+ and TpH- (orange) cells when the four DR subregions are considered collectively.

(e-g) Same as in (b-d), but experiments have been performed in ePET-Cre mice.
(h) Fluorescent image showing eYFP (green) and tyrosine-hydroxylase (TH) immunopositive (red) neurons in the DR, which is subdivided into four numbered subregions.
(i) Confocal images showing eYFP and TH-immunopositive neurons for the subregions delineated in (h). Vertical slice charts indicate percentage of eYFP-positive cells that co-express TH (eYFP+ TH+, blue) or lack expression of TH (eYFP+ TH-, orange) in individual DR subregions.
(j) Pie chart showing total percentage of eYFP+ and TH+ (blue) and eYFP+ and TH- (orange) cells when the four DR subregions are considered collectively.
(k-m) Same as in (h-j), but experiments have been performed in TH-Cre mice.
(n-p) Same as in (h-j), but experiments have been performed in PITX3-Cre mice.

Figure 2. Analysis of overlap between genetically identified DR cell populations.
(a) Schematic of experimental design showing viral injection into the DR of VGluT3-Cre mice.
(b) Confocal images showing anatomical distribution of DA (i.e., TH-immunopositive, blue), 5HT (TpH-imunopositive, red) and eYFP-positive (i.e., VGluT3-expressing, green) neurons in the DR (scale bar 0.5 mm). Note, the substantial overlap between eYFP and TpH in subarea #4 of the ventral DR.
(c) Confocal images showing eYFP (i.e., VGluT3-expressing, green) and TH-positive (blue) neurons for individual DR subregions. Vertical slice charts indicate percentage of eYFP-positive cells that co-express TH (eYFP+ TH+, blue) or lack expression of TH (eYFP+ TH-, orange) in individual DR subregions (scale bar 50 μm).
(d) Pie chart showing total percentage of eYFP+ and TH+ (blue) and eYFP+ and TH- (orange) cells when the four DR subregions are considered collectively.
(e) Confocal images showing eYFP (i.e., VGluT3-expressing, green) and TpH-positive (red) neurons for individual DR subregions. Vertical slice charts indicate percentage of eYFP-positive cells that co-express TpH (eYFP+ TpH+, blue) or lack expression of TpH (eYFP+ TpH-, orange) in individual DR subregions (scale bar 50 μm).
(f) Pie chart showing total percentage of eYFP+ and TpH+ (blue) and eYFP+ and TpH- (orange) cells when the four DR subregions are considered collectively.
(g) Schematic of experimental design showing viral injection into the DR of GAD2-Cre mice.
(h) Sample confocal images showing TH-immunopositive (blue) and eYFP-positive (i.e., GAD2-expressing, green) neurons in DR (scale bar 50 μm).

(i) Pie chart showing total percentage of eYFP+ and TH+ (blue) and eYFP+ and TH- (orange) cells when the four DR subregions are considered collectively.
(j) Schematic of experimental design showing viral injection into the DR of GAD2-Cre mice.
(k) Sample confocal images showing TpH-immunopositive (red) and eYFP-positive (i.e., GAD2-expressing, green) neurons in DR (scale bar 50 μm).
(l) Pie chart showing total percentage of eYFP+ and TpH+ (blue) and eYFP+ and TpH- (orange) cells when the four DR subregions are considered collectively.

Figure 3. Genetically defined DR cell populations are topographically organized and have different axonal projections.

Sample fluorescence images of eYFP-expressing DR cell bodies and eYFP-expressing axons terminals (green) in their respective target brain regions, as well as a schematic summarizing the topographical organization of genetically defined DR cell bodies and a qualitative evaluation of the strength of each projection (VTA: ventral tegmental area, LH: lateral hypothalamus, LHb: lateral habenula, MHb: medial habenula, Amy: amygdala, BLA: basolateral amygdala, CeL: central amygdaloid nucleus lateral division, CeM: central amygdaloid nucleus medial division , CeC: central amygdaloid nucleus capsular part, BNST: bed nucleus of stria terminalis, SEPT: septum, NAc: nucleus accumbens, aca: anterior commissure, PFC: prefrontal cortex) for different Cre-driver lines (TpH: red, TH: blue).

Figure 4. Whole-brain mapping of monosynaptic inputs onto DR neurons accessed via different transgenic mouse lines.

(a) Left: Schematic of viral injections for tracing of monosynaptic inputs to DR neurons using DAT-Cre, PITX3-Cre, SERT-Cre and ePET-Cre mice. Right: Fluorescence image showing GFP-positive cells in the ventral striatum before (left) and after automated segmentation by pixel intensity (middle, positive pixels in white). Segmented pixels were semi-automatically assigned to defined anatomical structures (right); e.g., dorsal striatum (DStr), ventral pallidum (VP), NAc medial shell (NAcMedS). Red arrow indicates a manually removed image artefact (right, scale bar: 1 mm).
(b) Graph showing high correlation between manually counted input neurons by a human observer and the automated segmentation procedure.
(c) Representative confocal images of DR starter cell populations in DAT-Cre (top) and PITX3-Cre (bottom) mice (green: RV-ΔG-GFP, red: TVA-mCherry, blue: TH; scale bars 50 μm). Starter cell populations in the VTA were defined as GFP- and TVA-mCherry-positive

cells. Bar graphs (right) show co-localization analysis of starter cells with TH (DAT-Cre: 82.4% TH-immunopositive, PITX3-Cre: 22.1% TH-immunopositive), non-starter (i.e., GFP-) TVA-mCherry-positive cells (DAT-Cre: 71.4% TH-immunopositive, PITX3-Cre: 26.3% TH-immunopositive) and secondary (TVA-mCherry-negative) cells (DAT-Cre: 21.3% TH-immunopositive, PITX3-Cre: 6.7% TH-immunopositive).
(d) Confocal images showing the anatomical distribution of DR starter cells in SERT-Cre (top) and ePET-Cre (bottom) mice (green: RV-ΔG-GFP, red: TVA-mCherry, blue: TpH; scale bars 50 μm). Bar graphs (right) show co-localization analysis of starter cells with TpH (SERT-Cre: 83.1% TpH-immunopositive, ePET-Cre: 70.3% TpH-immunopositive), non-starter (i.e., GFP-) TVA-mCherry-positive cells (SERT-Cre: 62.4% TpH-immunopositive, ePET-Cre: 71.8% TpH-immunopositive) and secondary cells (SERT-Cre: 19.5% TpH-immunopositive, ePET-Cre: 3.4% TpH-immunopositive).
(e) Bar graph showing quantification of inputs to DR neurons in PITX3-Cre (n = 3, light blue), DAT-Cre (n = 4, dark blue), SERT-Cre (n = 3, red) and ePET-Cre (n = 3, orange) mice. Data are presented as a percentage of total inputs (% pixels) counted in each individual brain. Inset shows a summary of input data pooled into major anatomical subdivisions indicated by dashed gray lines and labels. (Abbreviations: Olf Nuclei: anterior and accessory nuclei of the olfactory bulb, Claustrum: claustrum, Anterior Ctx: prelimbic, infralimbic, and orbitofrontal cortices, Motor Ctx: Motor Cortex, Piriform Ctx: piriform cortex, S.S. Ctx: Somatosensory cortex, Visual Ctx: visual cortex, Other Ctx: all other cortical areas not otherwise defined, NAcCore: nucleus accumbens core, NAcMedS: nucleus accumbens medial shell, NAcLatS: nucleus accumbens lateral shell, DStr: dorsal striatum, VP: ventral pallidum, GPe: globus pallidus external segment, GPi: globus pallidus internal segment, BNST: bed nucleus of the stria terminalis, SI: substantia innominate, CeM: central amygdaloid nucleus medial division , CeC: central amygdaloid nucleus capsular part, CeL: central amygdaloid nucleus lateral division, BLA: basolateral amygdala, DB: diagonal band, Septum: septum, PVA: paraventricular thalamic nucleus, MHb: medial habenula, LHb: lateral habenula, Other Thal: other thalamic areas not otherwise specified, PVH: paraventricular hypothalamic nucleus, LH: lateral hypothalamus, VMH: ventromedial hypothalamus, STh: subthalamic nucleus, MMB: mammillary body, PO: preoptic area, ZI: zona incerta, SN: substantia nigra, DpMe: deep mesencephalic nucleus, Sup. Col.: superior colliculus, PAG: periaqueductal gray, IPN: interpeduncular nucleus, MnR: median raphe, PPTg: pedunculopontine tegmental nucleus, LDTg: laterodorsal tegmental nucleus, PBN:

parabrachial nucleus, PnR: pontine reticular nucleus, RMg: raphe magnus nucleus) (* $p < 0.05$, ** $p < 0.01$; data represent means ± SEM).
(f) Horizontal and sagittal views of processed whole brains displaying brain-wide inputs to DR neurons in different transgenic mouse lines. Colors correspond to brain structures shown in (e).

Figure 5. Differences in monosynaptic inputs onto DA and 5HT DR neurons.
(a) Bar graph showing quantification of inputs onto DA (n = 4, dark blue) and 5HT (n = 6, yellow) DR neurons. DA group data is from DAT-Cre mice only to avoid off-target effects due to nonspecific Cre expression in PITX3-Cre mice. SERT-Cre and ePET-Cre lines were similarly cell-type specific for 5HT neurons, so this data was pooled for the 5HT group. Data are presented as a percentage of total input (% pixels) counted in each individual brain. Inset shows a summary of input data pooled into major anatomical subdivisions indicated by dashed gray lines and labels (* $p < 0.05$, ** $p < 0.01$; data represent means ± SEM).
(b) Graph showing principal components analysis for DA and 5HT DR groups.

Figure 6. Optogenetic dissection of the DR/PAG→CeA pathway.
(a) Schematic showing experimental design for retrograde labeling of CeA-projecting DR/PAG neurons using VGluT2-Cre mice. Inset shows injection-site of fluorescent retrobeads in the CeA (scale bar 0.5 mm).
(b) Analysis of co-localization between eYFP+ (i.e. VGluT2+) and TH+ (i.e. putatively dopaminergic) CeA-projecting cell populations in the DR/PAG (top) and the caudal linear nucleus (CLi, bottom). Left: Confocal image showing overview of the DR/PAG and CLi regions in VGluT2-Cre mice (scale bars 0.5 mm). Middle: Higher magnification images of the DR/PAG and CLi regions showing retrogradely labeled (beads, white) neurons. Note the prominent co-localization of eYFP (green) and TH-immunopositive (red) cells in the CLi. Right: Vertical slice charts showing percentage of retrogradely labeled and eYFP-positive cells that co-express TH (eYFP+ beads+ TH+, blue) or lack expression of TH (beads+ eYFP+ TH-, orange) in the DR/PAG and CLi regions (scale bars 50 μm).
(c) Pie chart showing total percentage of beads+ eYFP+ TH+ (blue) and beads+ eYFP+ and TH- (orange) cells when the anterior and posterior DR/PAG/CLi subregions are considered collectively.
(d) Schematic of experimental design to analyze functional connectivity of DR/PAG inputs to CeA neurons using DAT-Cre, TH-Cre and VGluT2-Cre mice.

(e) Sample traces from whole-cell recordings at -70 mV showing EPSCs generated by light stimulation of DR/PAG$_{VGLUT2}$ inputs to CeA neurons (red trace: sample of mean EPSC after CNQX application; scale bars: 20 pA/10 ms). Schematics shows localization of the recorded neurons in the CeA that responded (blue) and did not respond (gray) to light stimulation. Pie chart shows percentage of responders (blue) and non-responders (gray). Bar graph showing mean EPSC amplitudes for the cells that responded to light stimulation before (blue) and after (red) bath application of 10 μM CNQX (** $p < 0.01$; data represent means ± SEM).
(f, g) Same as in (e), but experiments were performed in TH-Cre (f) and DAT-Cre (g) mice.

SUPPLEMENTARY FIGURE LEGENDS

Supplementary Figure 1. Anatomical characterization of transgenic mouse lines in the median raphe nucleus and ventral tegmental area.
(a) Schematic of experimental design showing viral injection into the median raphe (MnR) of SERT-Cre mice.
(b) Confocal image showing co-localization of eYFP (green) and tryptophan-hydroxylase 2 (TpH) immunopositive (red) neurons in the MR, which is subdivided into three different subregions (scale bar 1 mm).
(c) Sample confocal images showing eYFP and TpH-positive neurons for the different areas delineated in (b). Vertical slice charts indicate percentage of eYFP-positive cells that co-express TpH (eYFP+ TpH+, blue) or lack expression of TpH (eYFP+ TpH-, orange) for individual MR subregions (scale bar 50 μm).
(d) Pie chart showing total percentage of eYFP+ and TpH+ (blue) and eYFP+ and TpH- (orange) cells when the three MnR subregions are considered collectively.
(e-h) Same as (a-d) but for anatomical characterization of ePET-Cre mice in the MnR.
(i) Schematic of experimental design showing viral injection into the ventral tegmental area (VTA) of PITX3-Cre mice.
(j) Regions of the rostral (r) and caudal (c) ventral midbrain in which eYFP/TH co-localization was analyzed.
(k, l) Representative fluorescence images of coronal brain slices showing TH-immunostaining (red) and eYFP-expression (green) in the caudal (k) and rostral (l) midbrain from a PITX3-Cre mouse (scale bar 1 mm).
(m, n) Confocal images showing TH-immunostaining (red) and eYFP-expression (green) for the different areas delineated in (k) and (l). Vertical slice charts indicate percentage of eYFP-

positive cells that co-express TH (eYFP+ TH+, blue) or lack expression of TH (eYFP+ TH-, orange) for individual VTA subregions (scale bar 50 μm).
(o-q) Pie charts showing the total percentage of co-localization of eYFP with TH-immunopositive (blue) or TH-immunonegative (orange) cells for the caudal (o), rostral (p) and for the entire ventral midbrain (q) for PITX3-Cre mice.

Supplementary Figure 2. Topography of genetically identified DR cell populations for individual mice.

Sample confocal images of the DR from three individual mice of each transgenic mouse line shown in Fig. 3 injected with AAV-DIO-eYFP. The leftmost image in each row (Mouse 1) corresponds to the DR image shown in Fig. 3 for comparison to DR images from Mouse 2 and Mouse 3. Note the consistent anatomical distribution patterns of genetically identified DR cell populations across mice from the same mouse line (eYFP: green, TH-immunostaining: blue, TpH-immunostaining: red; scale bars 0.5 mm).

Supplementary Figure 3. Projections of genetically identified DR cell populations to the amygdala.

Schematic showing projections of DR subpopulations to distinct amygdala subregions (vlPAG: ventrolateral periaqueductal gray, dDR: dorsal dorsal raphe, vlDR: ventrolateral dorsal raphe, vDR: ventral dorsal raphe, BLA: basolateral amygdala, CeL: central amygdaloid nucleus lateral division, CeM: central amygdaloid nucleus medial division, CeC: central amygdaloid nucleus capsular part.

Supplementary Figure 4. Control experiments for mapping monosynaptic inputs onto DR neurons.

(a) Schematic of viral injections into wildtype (C57Bl/6) mice.
(b) Sample fluorescence image of coronal brain slice showing very few GFP-positive cells in the DR. Note that subregion #1 contains two GFP-positive cells (scale bar 0.5 mm).
(c) Schematic of viral injections into SERT-Cre mice.
(d) Sample fluorescence image of coronal brain slice showing very few GFP-positive cells in the DR. Note that subregion #3 contains two GFP-positive cells (scale bar 0.5 mm).

Fig. 1 Cardozo Pinto et al.

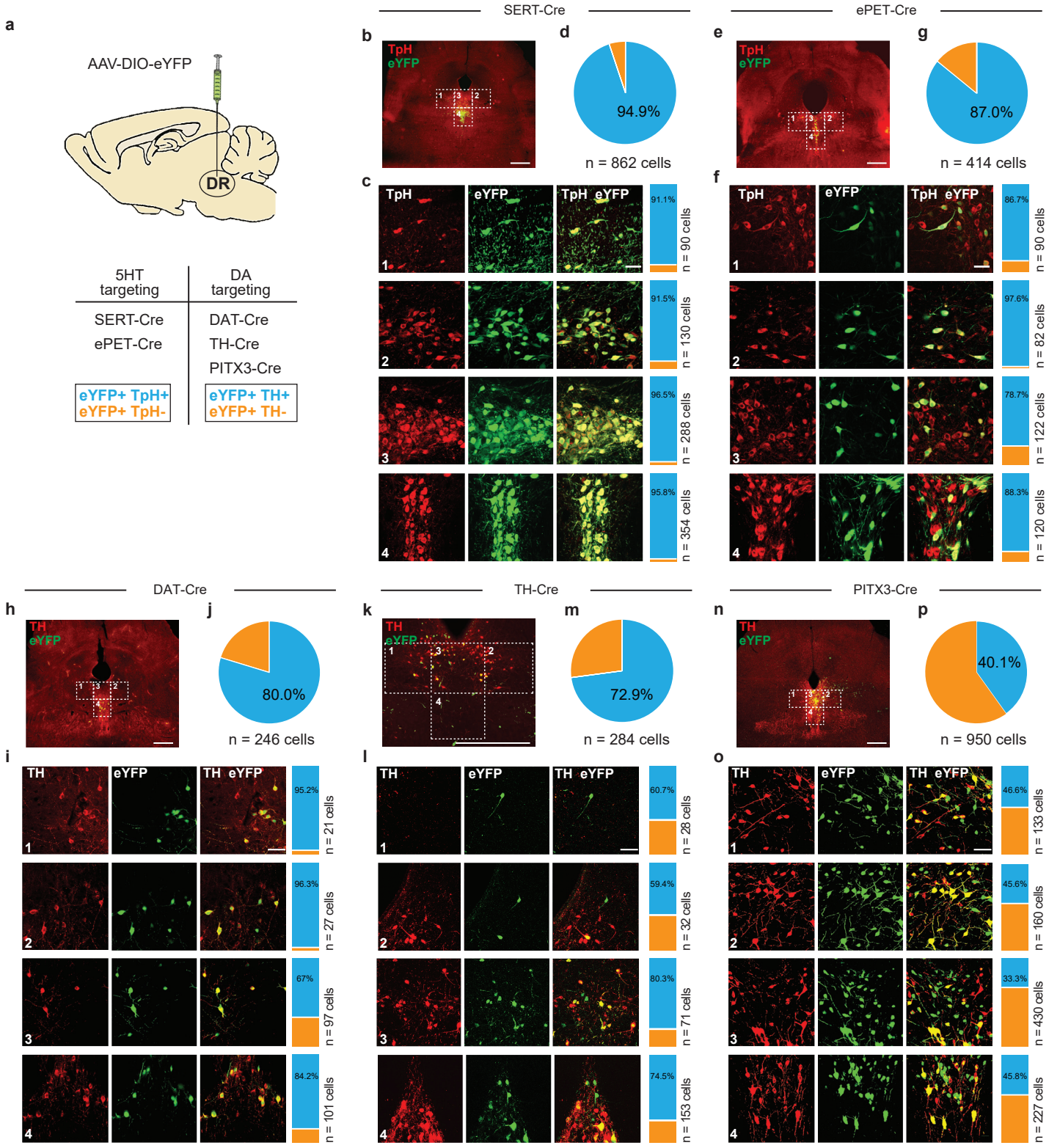

Fig. 2 Cardozo Pinto et al.

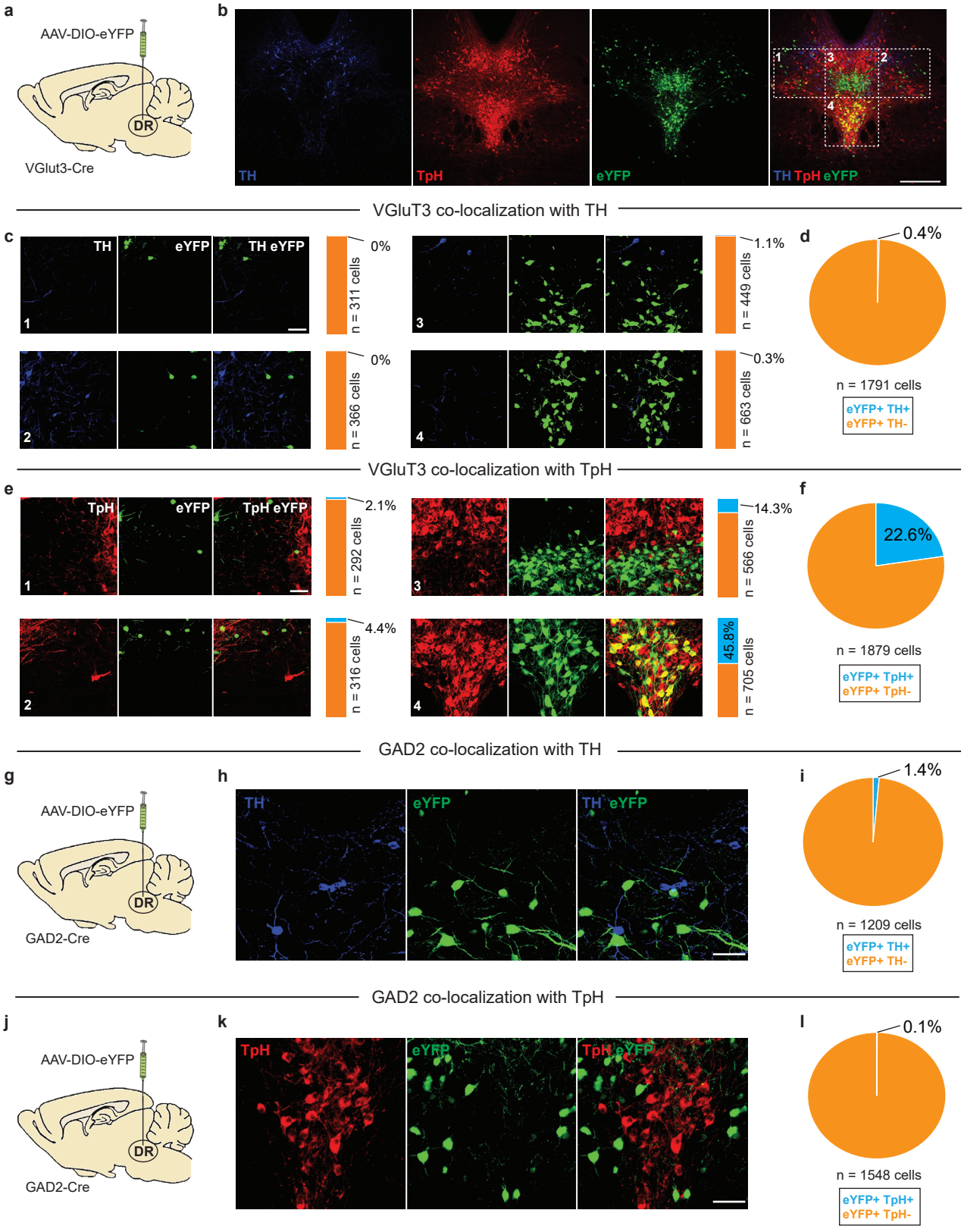

Fig. 3 Cardozo Pinto et al.

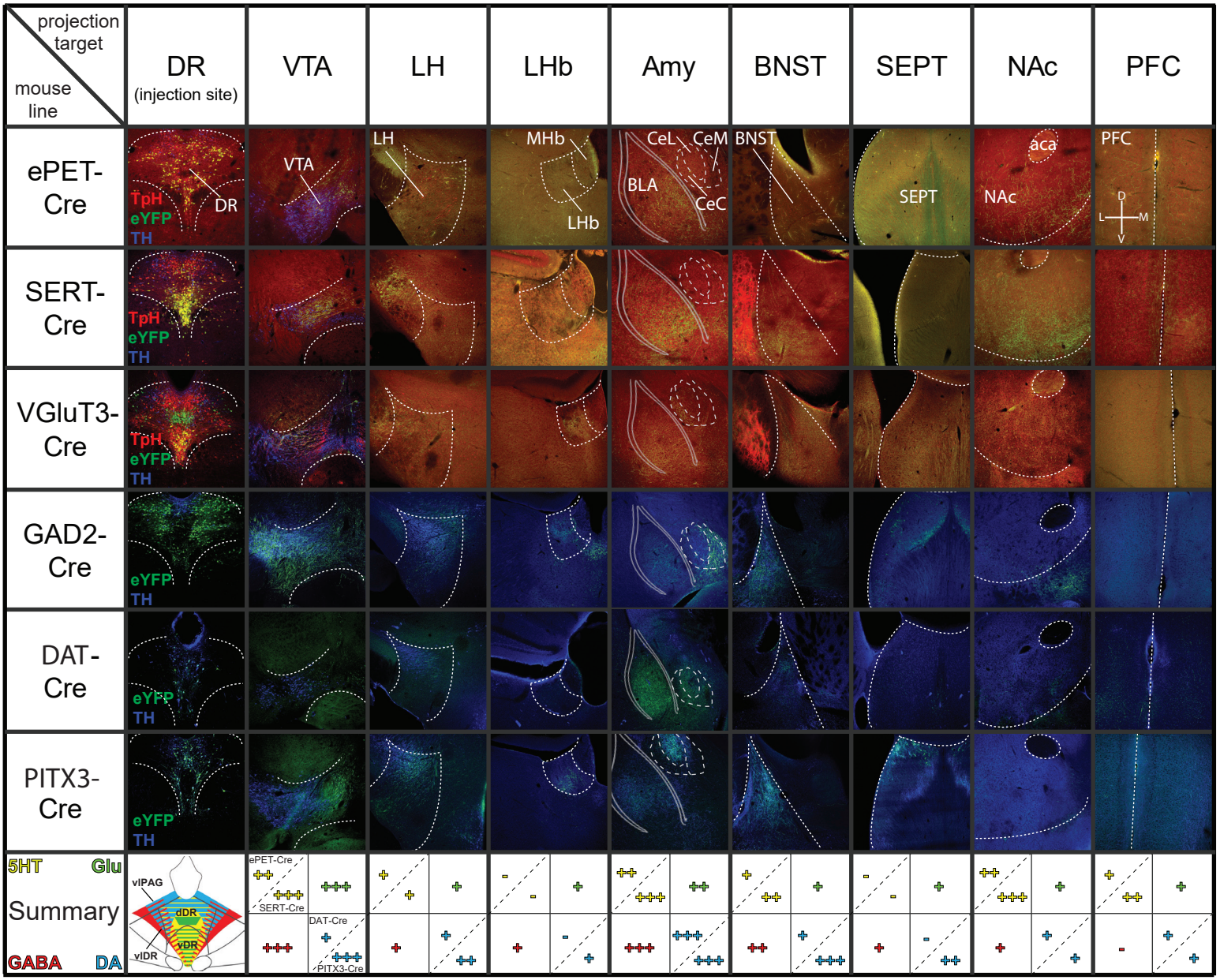

Fig. 4 Cardozo Pinto et al.

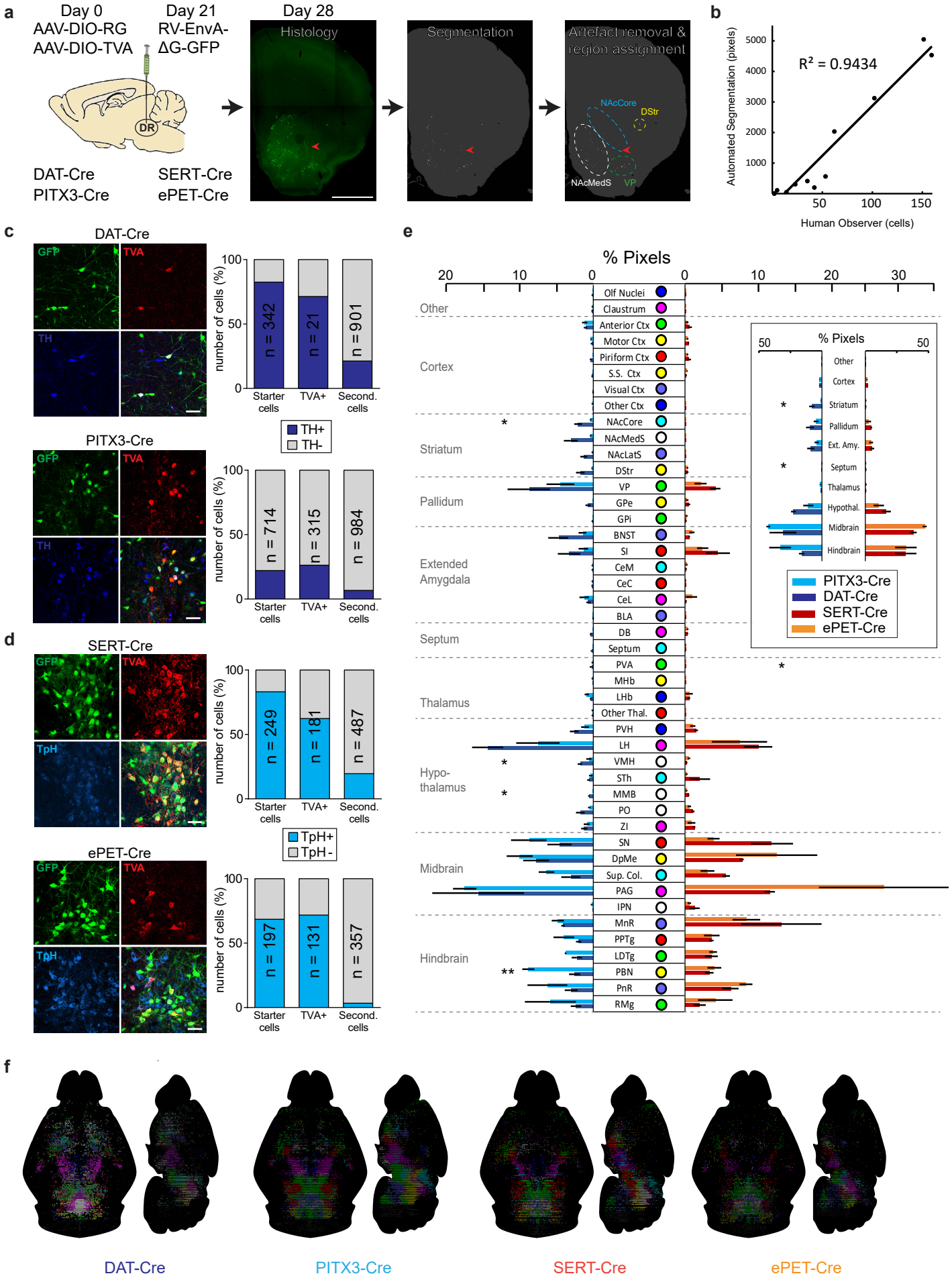

Fig. 5 Cardozo Pinto et al.

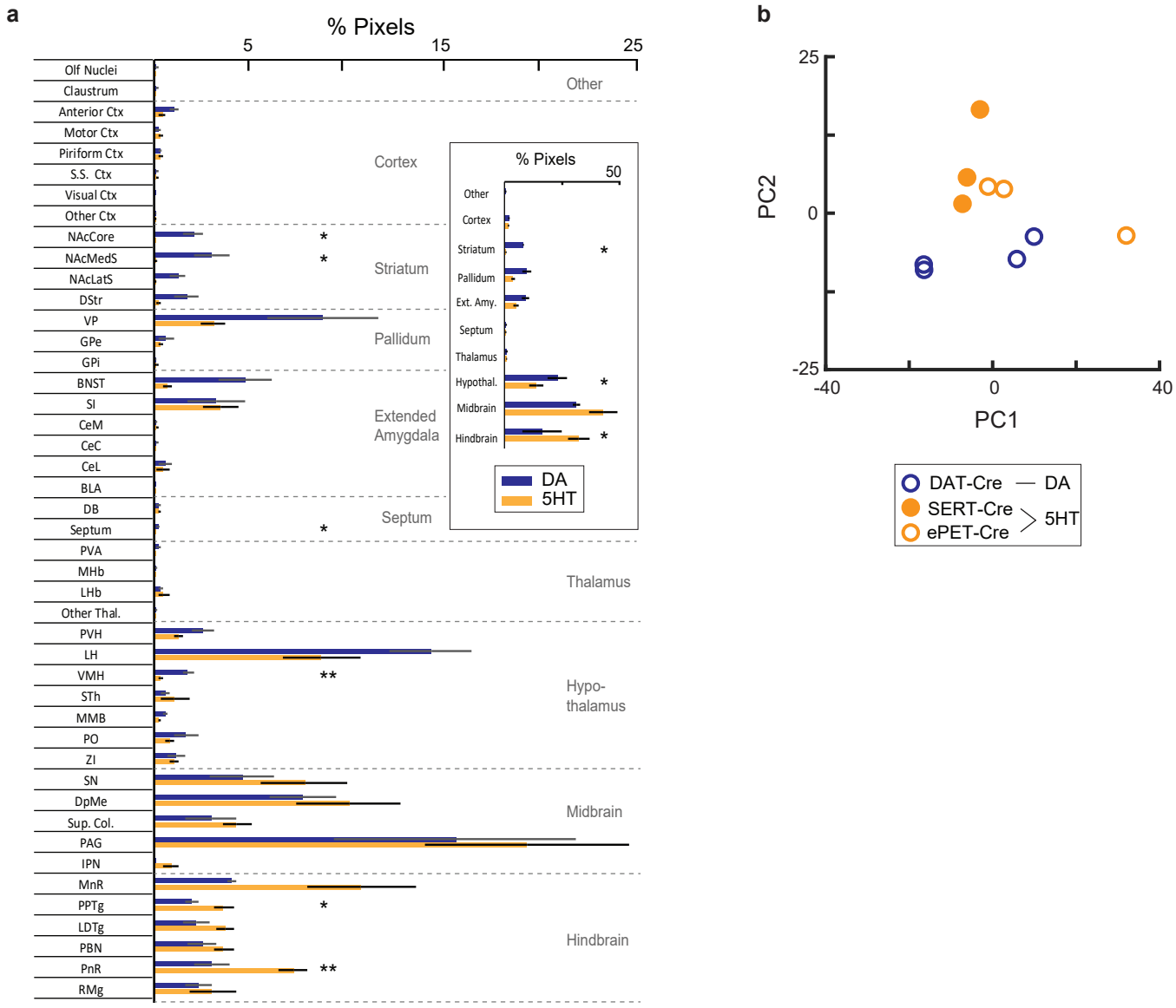

Fig. 6 Cardozo Pinto et al.

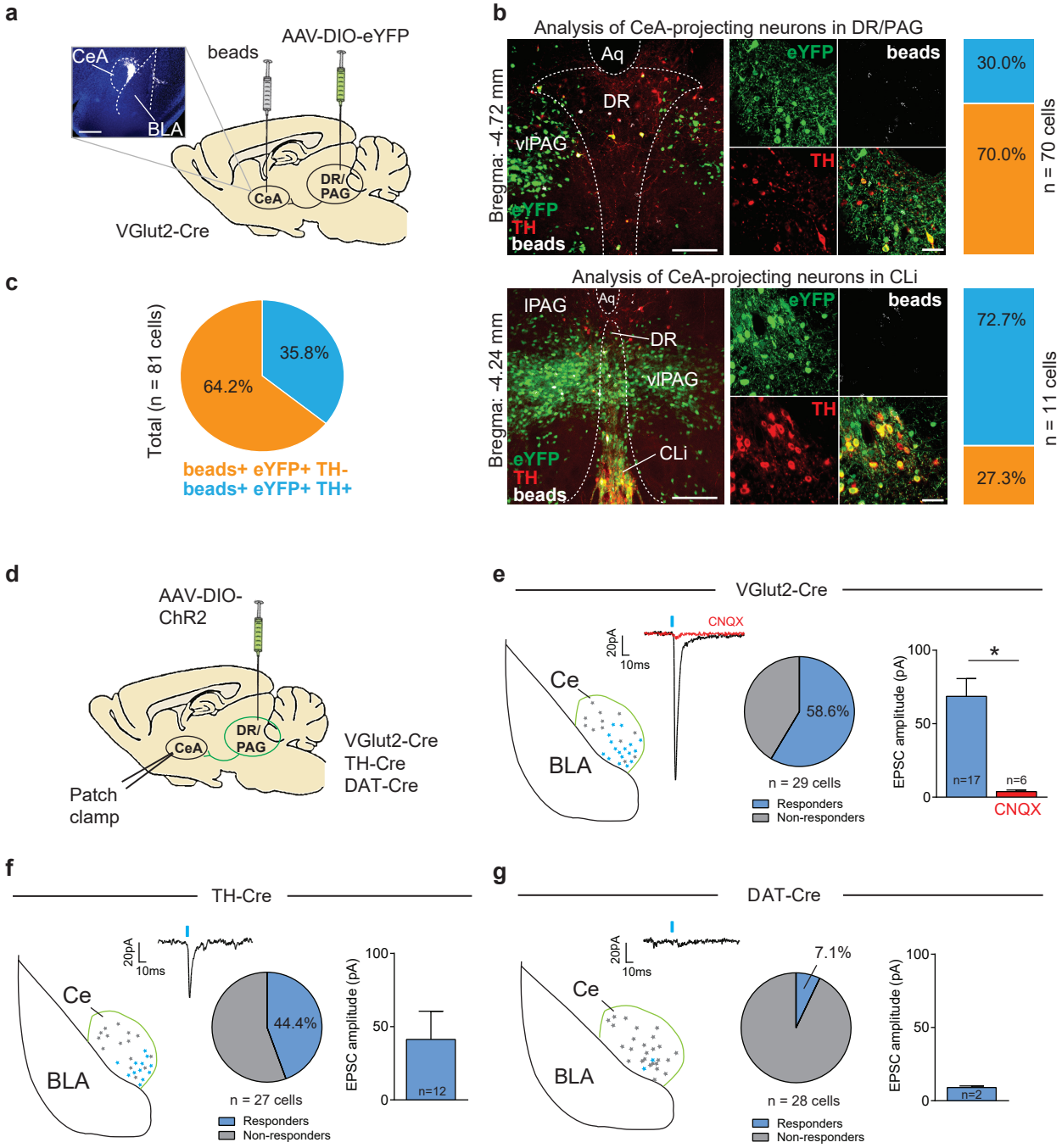

Fig. S1 Cardozo Pinto et al.

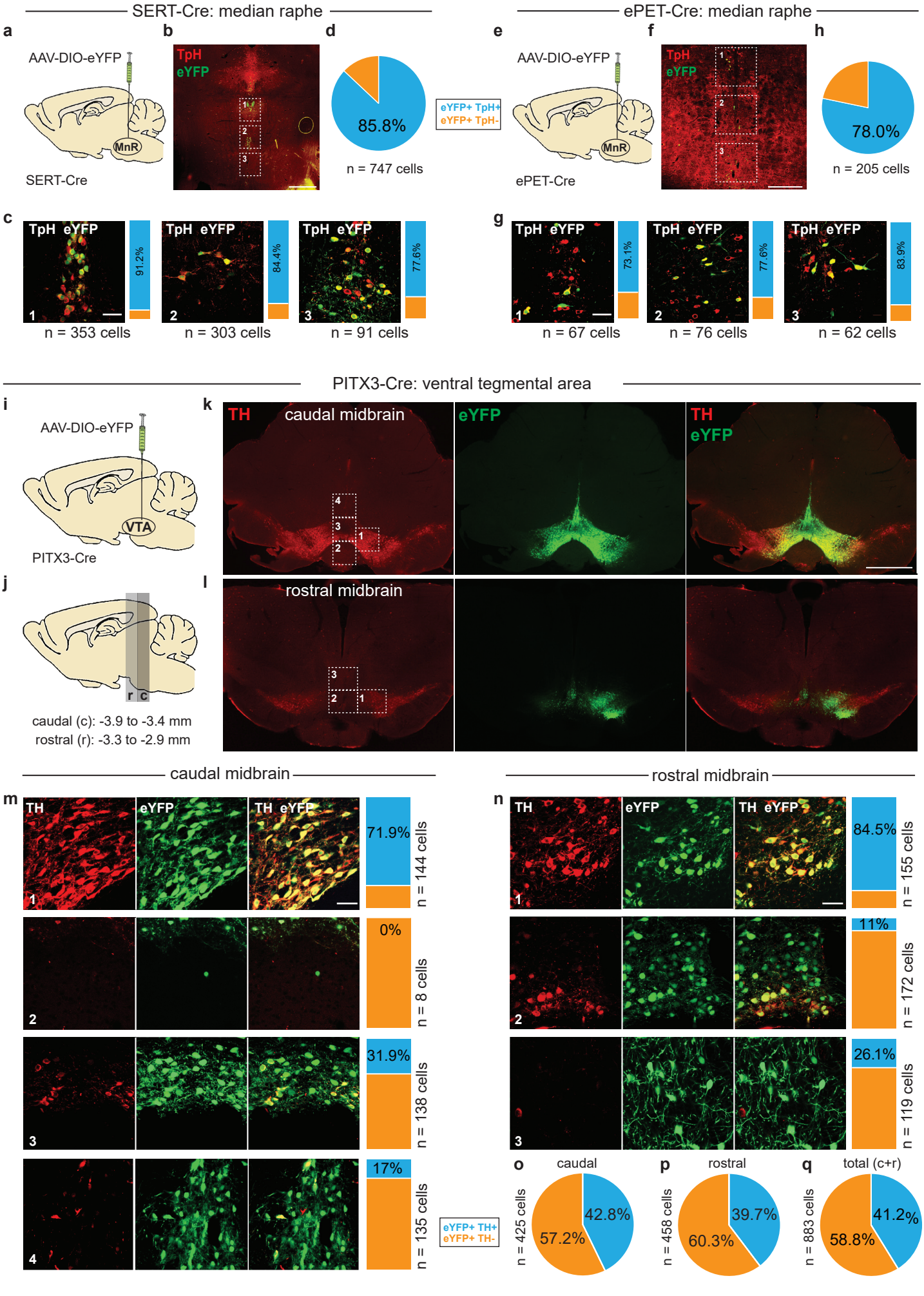

Fig. S2 Cardozo Pinto et al.

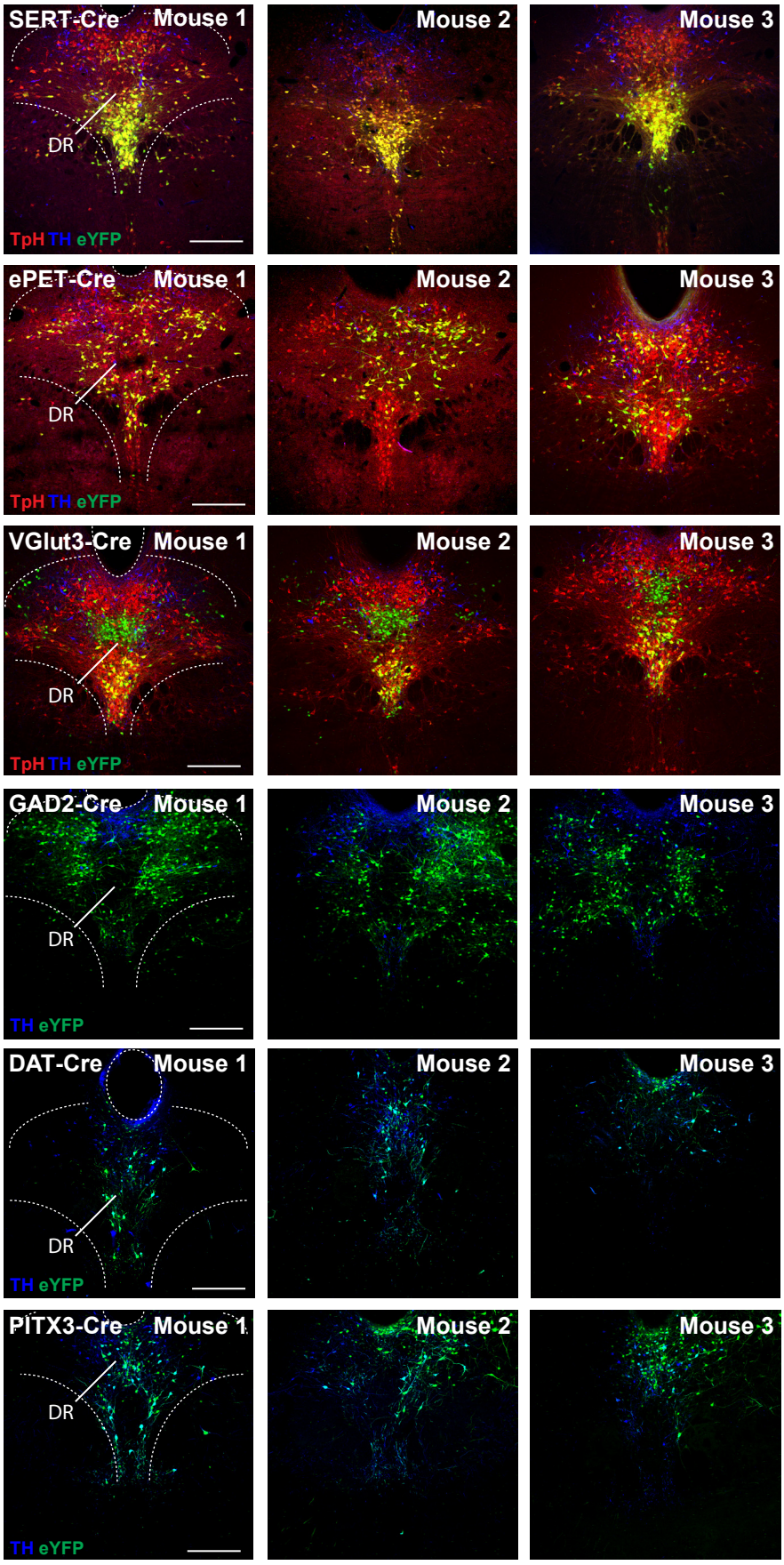

Fig. S3 Cardozo Pinto et al.

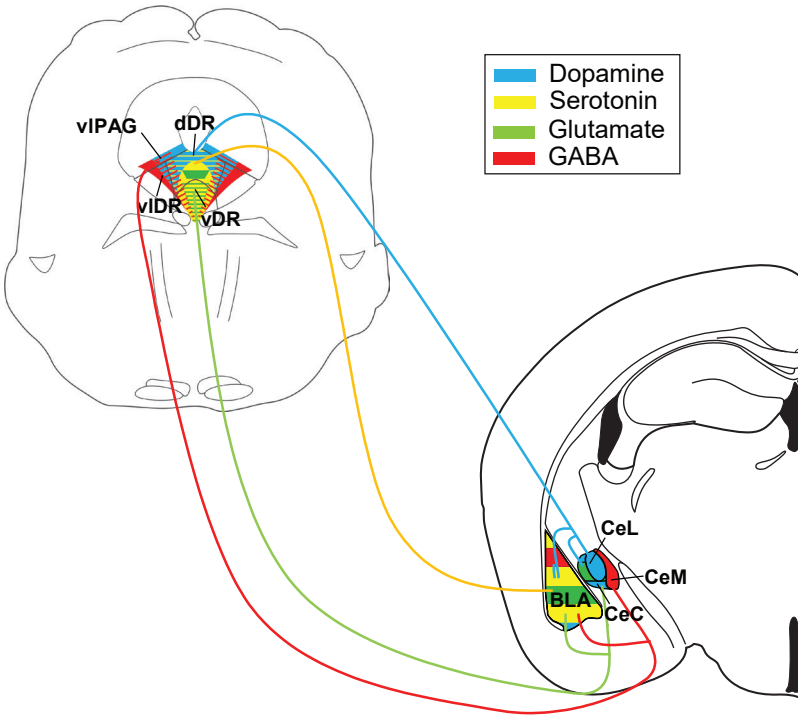

Fig. S4 Cardozo Pinto et al.